Annals of Operations Research (2024) 337:769–807
https://doi.org/10.1007/s10479-023-05686-8

ORIGINAL RESEARCH

A robust route to randomness in a simple Cournot duopoly game where ambiguity aversion meets constant expectations

D. Radi[1,2] · **L. Gardini**[3] · **D. Goldbaum**[4]

Received: 31 January 2023 / Accepted: 24 October 2023 / Published online: 16 November 2023

Abstract
In this paper we investigate the dynamics of a duopoly game with ambiguity aversion regarding uncertainty in demand and constant expectations concerning competitor production. The focus is on an asymmetric Cournot game where players engage in robust optimization and have different beliefs about the possible realizations of the random parameters of the price function. The players' ambiguity aversion introduces multiple equilibria and instability that otherwise would not be present. The investigation of the global dynamics of the game reveals the emergence, through border-collision bifurcations, of periodic and chaotic dynamics.

Keywords Cournot duopoly · Ambiguity aversion · Constant expectations · Piecewise linear maps · Border collision bifurcations

1 Introduction

The lack of trust in a unique probabilistic description of a random event is known as Knightian uncertainty. This uncertainty impacts on the decision process of agents that can be motivated in terms of ambiguity aversion, see Ellsberg (1961). Ambiguity aversion can be modeled in terms of maximin preferences, see, e.g., Gilboa and Schmeidler (1989), that degenerate in the worst-case approach to uncertainty, or robust optimization, when the lack of trust involves all possible probability distributions over a finite set of possible realizations. A game where ambiguity regards the slopes of the inverse demand functions and players are engaged in robust optimization is proposed and analyzed in Aghassi and Bertsimas (2006), Crespi et al. (2017) and Crespi et al. (2023). Employing this modeling framework, Crespi et al. (2023) show that ambiguity aversion modifies the Cournot–Nash equilibria of a duopoly game. See,

✉ D. Radi
davide.radi@unicatt.it

1 DiMSEFA, Catholic University of the Sacred Heart, Via Necchi 9, 20123 Milan, Italy

2 Department of Finance VŠB, Technical University of Ostrava, Ostrava, Czech Republic

3 Department of Economics, Society and Politics, University of Urbino Carlo Bo, Urbino, Italy

4 Economics Discipline Group, University of Technology Sydney, Sydney, NSW, Australia

e.g., Malueg and Tsutsui (1996), Malueg and Tsutsui (1998), Xu (2010) and Lepore (2012) for similar assumptions regarding an uncertain market demand.

Recently, Radi and Gardini (2023) make a step further in this direction by considering a symmetric duopoly game where ambiguity aversion is combined with constant expectations concerning competitor production. A piecewise linear map, given by a bi-modal best-reply function, describes the output dynamics generated by this model which is known as the Cournot-tâtonnement process. By perturbing the configuration of the uncertainty set, the investigation of the global dynamics of the map reveals an abrupt transition from a globally stable Cournot–Nash equilibrium to chaotic dynamics. Thus, showing for the first time that chaotic dynamics can emerge even in a very simple and stylized duopoly with linear demand functions and constant marginal costs of production.

The analysis in Radi and Gardini (2023) is limited to a symmetric duopoly game and shows that chaotic dynamics emerges when the uncertainty set of firms includes a realization of the random parameters that implies an oligopoly game with more than two competitors. In this paper, we generalize the modeling framework by considering a duopoly where firms have different beliefs about the uncertainty set. A firm relies on an uncertainty set made of two realizations that are worst-case depending on the quantities produced by the two firms, while, as opposed to Radi and Gardini (2023), the other firm relies on an uncertainty set made by a unique worst-case realization of the values of the random parameters that define the inverse-demand function.

As in Radi and Gardini (2023), the Cournot-tâtonnement process is described by a decoupled square two-dimensional system that reduces to the study of a one-dimensional map. Differently from Radi and Gardini (2023), the one-dimensional map that describes the global dynamics of the model is not the decreasing-increasing-decreasing best-reply function but it is made of up to five branches and the Cournot–Nash equilibria can be more than three and up to five. These differences are reflected in a wider variety of nonlinear dynamics for the asymmetric game, which include attracting cycles coexisting with locally-asymptotically-stable Cournot–Nash equilibria, superstable periodic solutions, multiple chaotic attractors coexisting with locally-asymptotically stable Cournot–Nash equilibria and, finally, chaotic repellors coexisting with locally-asymptotically-stable Cournot–Nash equilibria.

All in all, the investigation of the dynamics of the asymmetric game reveals that chaotic dynamics can emerge by perpetuating the configuration of the uncertainty sets, which is consistent with the results in Radi and Gardini (2023). Additionally, the asymmetric game extends for the first time the chaotic region to the set of parameter values considered in the duopoly game by Singh and Vives (1984), i.e. to a parameter constellation consistent with a single opponent. This proves the robustness of the route to randomness obtained by mixing ambiguity aversion and non-perfect foresight expectations. Such a randomness raises volatility in the levels of productions, prices and profits. This may have several economic implications in terms of consumer choices, types and levels of investments and financial sustainability of the duopoly, see, e.g., Minton and Schrand (1999), Comin and Mulani (2009), Czarnitzki and Toole (2011) and Nocetti and Smith (2011).

The current paper enriches the literature on chaotic Cournot duopoly started with the seminal contribution of Rand (1978). It shows that ambiguity introduces nonlinearity in an otherwise linear duopoly and this nonlinearity combined with constant expectations leads to chaos. Chaotic dynamics is generated despite a very simple market setup and a very simple configuration of the set of realizations of random parameters.

The road map of the paper is the following. Section 2 introduces the duopoly game with ambiguity aversion. Section 3 contains preliminary results about existence and stability of Cournot–Nash equilibria. Section 4 contains the bifurcation analysis mainly focused on two-

dimensional bifurcation diagrams. Section 5 comments on the economic implications of the main findings of the bifurcation analysis. Section 6 concludes. A summary of those results on decoupled square two-dimensional systems (employed in the analysis) are recap in Appendix A for the sake of completeness.

2 A duopoly game with players engaged in robust optimization

Consider an oligopoly populated by two firms producing two differentiated products as in Singh and Vives (1984). Let q_1 be the quantity of product 1 produced by firm 1 and let q_2 be the quantity of product 2 produced by firm 2.

All produced products of type 1 and 2 are sold in the market at the following prices

$$\begin{aligned} P_1(q_1, q_2) &= \max\{a_1 - b_1 q_1 - \gamma q_2; 0\} \quad \text{and} \\ P_2(q_1, q_2) &= \max\{a_2 - \gamma q_1 - b_2 q_2; 0\} \end{aligned} \tag{1}$$

respectively. For every $i \in \{1, 2\}$, the choke price a_i is assumed to be constant over time and its value is known to firm i. Similarly to Malueg and Tsutsui (1996), Malueg and Tsutsui (1998) and Xu (2010), the remaining parameters $b_1 > 0$, $b_2 > 0$ and $\gamma > 0$ are instead random variables in order to capture, for example, consumers' tastes that change over time. Firms are in complete ignorance as to how these random variables are distributed and have their own belief about the set of possible realizations.[1]

To accommodate this type of uncertainty and firms' heterogeneous beliefs about the possible realizations of the unknown parameters, the inverse-demand functions are rewritten as follows

$$\begin{aligned} P_1(q_1, q_2; b_1, \gamma_1) &= \max\{a_1 - b_1 q_1 - \gamma_1 q_2; 0\} \quad \text{and} \\ P_2(q_1, q_2; b_2, \gamma_2) &= \max\{a_2 - \gamma_2 q_1 - b_2 q_2; 0\} \end{aligned} \tag{2}$$

where $\gamma_1 \neq \gamma_2$ captures the firm's heterogeneous beliefs on the possible realizations of the random parameters.

To complete the model, we assume constant marginal costs of production for both firms:

$$C_1(q_1) = c_1 q_1 + \delta_1 \quad \text{and} \quad C_2(q_2) = c_2 q_2 + \delta_2 \tag{3}$$

where the marginal cost c_i, as well as the fixed cost δ_i, is assumed to be known to firm i, with $i = 1, 2$. Then, the profit functions of firm 1 and firm 2 are

$$\begin{aligned} \Pi_1(q_1, q_2; b_1, \gamma_1) &= P_1(q_1, q_2; b_1, \gamma_1)\, q_1 - C_1(q_1) \quad \text{and} \\ \Pi_2(q_1, q_2; b_2, \gamma_2) &= P_2(q_1, q_2; b_2, \gamma_2)\, q_2 - C_2(q_2) \end{aligned} \tag{4}$$

respectively.

Here, the setup in Singh and Vives (1984) is generalized by assuming ambiguity on b_1, b_2, γ_1 and γ_2 that results in the lack of trust in any probability distribution over a support set U_i, $i = 1, 2$, representing firm i's beliefs on the true set U_i^* of possible realizations of the values of parameters (b_i, γ_i). As in Radi and Gardini (2023), firms are averse to uncertainty and this ambiguity aversion mirrors in the worst-case approach to uncertainty (maximin preferences), see, e.g., Wald (1945), Gilboa and Schmeidler (1989) and Aghassi and Bertsimas (2006). According to the worst-case approach to uncertainty, a player is engaged

[1] Malueg and Tsutsui (1996), Malueg and Tsutsui (1998) and Xu (2010) consider instead a (Bayesian) duopoly model with risk-neutral firms that know the distribution of the random parameters.

in robust optimization and maximizes the guaranteed payoff, see, e.g., Ben-Tal et al. (2009).[2] Therefore, the player computes for each possible combination of q_1 and q_2 the minimum payoff that can be obtained based on the possible realizations of the unknown values of the parameters, which is the guaranteed payoff. Then, given the output of the competitor, a player selects its level of production in order to maximize this guaranteed payoff.[3]

A key element in robust optimization is the uncertainty set. As in Radi and Gardini (2023), we assume that firm i has conservative belief U_i about the true uncertainty set U_i^*, that is $U_i \supseteq U_i^*$ for $i = 1, 2$. Then, the maximum-guaranteed payoff computed according to U_i is never higher than the one computed according to U_i^*. A conservative belief U_i is also a consistent belief, that is a firm cannot exclude this uncertainty set based on historical observations.[4] As opposed to Radi and Gardini (2023), instead, we assume asymmetric beliefs on uncertainty sets. Noting that a realization of the values of the parameters may or may not be a worst-case realization depending on firms' output q_1 and q_2 and noting that worst-case realizations are the only ones that impact on the output of the game, we neglect realizations that cannot be worst-case. Moreover, we assume that firm 1 relies on an uncertainty set made of two (possible) worst-case realizations: $U_1 = \left\{\left(\overline{b}_1, \underline{\gamma}_1\right), \left(\underline{b}_1, \overline{\gamma}_1\right)\right\}$. Instead, firm 2 relies on an uncertainty set made of a unique worst-case realization: $U_2 = \{(b_2, \gamma_2)\}$.[5] Then, the best-reply function of firm 1 is given by

$$R_1(q_2) = \underset{q_1 \geq 0}{\operatorname{argmax}} \left[\min_{(b_1, \gamma_1) \in U_1} \Pi_1(q_1, q_2; b_1, \gamma_1) \right] \tag{5}$$

while the best-reply function of firm 2 is given by[6]

$$R_2(q_1) = \underset{q_2 \geq 0}{\operatorname{argmax}} \Pi_2(q_1, q_2; b_2, \gamma_2) \tag{7}$$

[2] Indeed, in optimization theory, the worst-case approach to uncertainty corresponds to the robust optimization, see Soyster (1973), Ben-Tal et al. (2009) and Bertsimas et al. (2011). See also Keith and Ahner (2021) for an overview of decision theory and optimization under uncertainty.

[3] This is a very conservative approach to uncertainty that in game theory goes back to von Neumann and Morgenstern (1947) and to the minimax principle as an optimality principle for a two-person zero-sum game. Specifically, minimax principle expresses the desire of each player to obtain the largest sure pay-off, therefore, adopting a robust-optimization approach to uncertainty. This approach to uncertainty reflects ambiguity aversion, see Ellsberg (1961), in case of complete ignorance as to how the random parameters are distributed, see Wald (1945).

[4] Dealing with a dynamic adjusted process, a belief U_i on the uncertainty set U_i^* turns out to be wrong when a past profit realization is not consistent with any of the parameter realizations in U_i and with the observed levels of production. This possibility is excluded when $U_i \supseteq U_i^*$ and the consistency with the historical observations is therefore guaranteed.

[5] Let us point out that to study the sensitivity of a solution of a robust optimization problem to the level of uncertainty, Crespi et al. (2018) and Rocca (2022) adopt a representation of the uncertainty set based on the following parametrization $W_i = (1 - \lambda)\hat{U}_i + \lambda U_i$, where $\lambda \in [0, 1]$, $\hat{U}_i \subset U_i$ is a singleton and U_i is a closed and bounded subset of $\mathbb{R}^v$. Here, v is the number of parameters generating uncertainty. Increasing λ is equivalent to increase the level of uncertainty, ranging from no uncertainty ($\lambda = 0$) to the case of $W_i = U_i$ ($\lambda = 1$). In game theory, Crespi et al. (2023) adopt the same representation of the uncertainty set to study analogies and differences between the solutions of a game with uncertainty and those of the same game but without uncertainty. We avoid this type of representation as it is not useful to the scope of the current paper, which is to analyze the global dynamics of the duopoly game for different configurations of U_i (not only for different levels of uncertainty).

[6] Note that whenever there is a unique worst-case realization, that is, U_2 is a singleton, then

$$\min_{(b_2, \gamma_2) \in U_2} \Pi_2(q_1, q_2; b_2, \gamma_2) = \Pi_2(q_1, q_2; b_2, \gamma_2) \quad \forall q_1, q_2 \tag{6}$$

Therefore, we can neglect the min operator in (7).

The analytical expressions of the best-reply functions (5) and (7) are derived under the following parameter restrictions.

Assumption 1 Consider: $\overline{b}_1 > \underline{b}_1 \geq 0$, $b_2 > 0$, $\gamma_2 \geq 0$, $\overline{\gamma}_1 > \underline{\gamma}_1 \geq 0$, $a_1 > 0$ and $a_2 > 0$.

Then, solving problems (5) and (7) under Assumption 1, we obtain

$$R_1(q_2) = \begin{cases} \frac{a_1 - c_1}{2\overline{b}_1} - \frac{\underline{\gamma}_1}{2\overline{b}_1} q_2 & \text{if} \quad \underline{q}_2 > q_2 \geq 0 \\ \frac{\overline{\gamma}_1 - \underline{\gamma}_1}{\overline{b}_1 - \underline{b}_1} q_2 & \text{if} \quad \overline{q}_2 \geq q_2 \geq \underline{q}_2 \\ \frac{a_1 - c_1}{2\underline{b}_1} - \frac{\overline{\gamma}_1}{2\underline{b}_1} q_2 & \text{if} \quad q_2^M > q_2 > \overline{q}_2 \\ 0 & \text{if} \quad q_2 \geq q_2^M \end{cases} \tag{8}$$

with

$$\underline{q}_2 = \frac{(a_1 - c_1)\left(\overline{b}_1 - \underline{b}_1\right)}{\underline{\gamma}_1\left(\overline{b}_1 - \underline{b}_1\right) + 2\overline{b}_1\left(\overline{\gamma}_1 - \underline{\gamma}_1\right)} \tag{9}$$

$$\overline{q}_2 = \frac{(a_1 - c_1)\left(\overline{b}_1 - \underline{b}_1\right)}{\overline{\gamma}_1\left(\overline{b}_1 - \underline{b}_1\right) + 2\underline{b}_1\left(\overline{\gamma}_1 - \underline{\gamma}_1\right)} \tag{10}$$

$$q_2^M = \frac{a_1 - c_1}{\overline{\gamma}_1} \tag{11}$$

(note that $q_2^M > \overline{q}_2 > \underline{q}_2$ always) and

$$R_2(q_1) = \begin{cases} \frac{a_2 - c_2}{2b_2} - \frac{\gamma_2}{2b_2} q_1 & \text{if } q_1^M > q_1 \geq 0 \\ 0 & \text{if } q_1 \geq q_1^M \end{cases} \tag{12}$$

with

$$q_1^M = \frac{a_2 - c_2}{\gamma_2} \tag{13}$$

The game is played at any time $t \in \mathbb{N}$. Then, given firm 1's next-period expected level of production of firm 2, which is denoted by $q_2^e(t+1)$, and given firm 2's next-period expected level of production of firm 1, which is denoted by $q_1^e(t+1)$, the quantity dynamics of the Cournot game is defined as follows

$$(q_1(t+1), q_2(t+1)) = T\left(q_1^e(t+1), q_2^e(t+1)\right) \tag{14}$$

where

$$T\left(q_1^e(t+1), q_2^e(t+1)\right) := \left(R_1\left(q_2^e(t+1)\right), R_2\left(q_1^e(t+1)\right)\right) \tag{15}$$

To close the model, we assume that firms have constant expectations (instead of perfect expectations requiring the complete-information model in Singh and Vives (1984)) about the level of production of the competitors, that is, $q_1^e(t+1) = q_1(t)$ and $q_2^e(t+1) = q_2(t)$ for all t. It follows that the quantity dynamics of the Cournot game is given by the following map

$$(q_1(t+1), q_2(t+1)) = T(q_1(t), q_2(t)) \tag{16}$$

where $T(q_1(t), q_2(t)) = (R_1(q_2(t)), R_2(q_1(t)))$.

Relaxing the complete-information hypothesis by considering a constant expectation scheme, we allow $q_i^e(t) \neq q_i(t)$, for $i = 1, 2$.[7] Therefore, the quantity-expectation space

[7] Of course, $q_i(t) = q_i^e(t)$ when $q_i(t)$ is an equilibrium value or stationary solution.

does not necessarily coincide with the action space of the game and map T generates a so-called Cournot-tâtonnement process. Differently from a repeated game framework, this dynamic game process hides a form of naivety well-known in behavioral economics, see Hammond (1976); Machina (1989); Rubinstein (1991) and Hey and Lotito (2009), i.e. time inconsistency in decision making which, in the case of Rubinstein (1991), manifests as firms ignoring the effects of their own behavior on the future production choices of the opponents. As discussed in Mamatame and Tse (1981), this naivety is justified by players that lack information of the objective functions of other players. Moreover, this naivety results in firms that are engaged in robust optimization in the quantity-expectation space but they are not so in the action space.

The implications of this behavior inconsistency will be discussed in the following. In preparation, let us clarify some assumptions that are implicit in the modeling choices. Specifically, the best reply behavior is consistent with the hypothesis that: (1) players know the own cost function; (2) players know the form of the own inverse demand function; (3) players know that the slopes of the own inverse demand are random variables; (4) players know the set of all possible realizations of these random parameters; (5) players know how to calculate a best reply. Further, constant expectations imply that, though they observe the opponent's output from the previous period; (6) players have incomplete information of others' objectives. Moreover, the worst-case approach to uncertainty implies that: (7) players are in complete ignorance of the distribution of the random parameters of their inverse demand functions; (8) players are averse to uncertainty.[8] Finally, we assume that: 9) players do not know the last-period profit of the opponent. Although this last assumption is not strictly required to justify the myopic best-reply behavior, experiments conducted in Huck et al. (1999) show that when subjects know individual profits (in addition to the true market structure), their quantity adjustments go significantly towards the most successful strategy of the previous period (imitation process, see, e.g., Vega-Redondo (1997)) instead of depending significantly on the myopic best reply.

Let us also point out that the firms have access to the history of the public market information of output and price and the firm's own private profit. However, firms do not observe the realizations of the random parameters. This limited information does not allow player inference about the realized value of the random variables nor the distribution from which the random parameters are drawn. Therefore, history does not alter the players' perception of the uncertainty set.

As a final remark on the modeling setup, let us underline that the robust-optimization approach to uncertainty negates the probability distribution from the decision process and, as discussed in Aghassi and Bertsimas (2006), leads to a distribution-free solution concept in game theory, i.e. robust-optimization equilibria that in the following will be denoted Cournot–Nash equilibria with an abuse of terminology. In particular, uncertainty has a deterministic representation in terms of sets of all possible realizations of the random parameters and the optimization process is therefore deterministic, see Ben-Tal et al. (2009). It follows that the output dynamics of the Cournot-duopoly model is also deterministic.[9] As the attention is limited to global dynamics of the output of the model, we do not need to specify the probability

[8] The worst-case approach to uncertainty is justified when agents are uncertainty averse, as shown in Ellsberg (1961), and have no information regarding the probability distribution of the random parameters, see, e.g., Wald (1945) and Keith and Ahner (2021).

[9] Differently from the output dynamics that is deterministic, profits and prices depend on the random variables (random parameters) that define the inverse demand function and are random themselves. Therefore, to study the dynamics of profits and prices is required to specify the probability distribution of the random parameters. The dynamics of profits and prices are neglected in the current paper.

distribution of the random parameters. Specifically, the results that follow about the quantity dynamics of the duopoly are valid for random parameters with any probability distribution as long as all their realizations (at least the subset given by worst-case realizations) are included in the uncertainty sets that are assumed.[10]

3 Cournot–Nash equilibria and local stability

Describing the time-evolution of the quantity dynamics of the Cournot-duopoly model, map T is a decoupled square two-dimensional dynamical system, see Bischi et al. (2000). Then, a specific one-dimensional map, that will be denoted by F, can be considered instead of the two-dimensional map T to investigate the global dynamics of T itself. In the following, we first show how to derive this one-dimensional map and then we classify its equilibria, we derive conditions for their local asymptotic stability and, finally, we study its global dynamics.

Set $x = q_1$, $y = q_2$ and $a = a_1 - c_1 = a_2 - c_2$, and let us rewrite the best-reply functions (17) and (19) as follows:

$$R_1(y) = \begin{cases} f_1(y) := \mu_L - s_L y & \text{if} \quad y_L > y \geq 0 \\ f_2(y) := ry & \text{if} \quad y_U > y \geq y_L \\ f_3(y) := \mu_U - s_U y & \text{if} \quad y_M > y \geq y_U \\ f_4(y) := 0 & \text{if} \quad y \geq y_M \end{cases} \tag{17}$$

where

$$\begin{gathered} \mu_L = \frac{a}{2\overline{b}_1}; \quad s_L = \frac{\underline{\gamma}_1}{2\overline{b}_1}; \quad r = \frac{\overline{\gamma}_1 - \underline{\gamma}_1}{\overline{b}_1 - \underline{b}_1}; \quad \mu_U = \frac{a}{2\underline{b}_1}; \quad s_U = \frac{\overline{\gamma}_1}{2\underline{b}_1}; \\ y_L = \frac{\mu_L}{s_L + r}; \quad y_U = \frac{\mu_U}{s_U + r}; \quad y_M = \frac{a}{\overline{\gamma}_1} \end{gathered} \tag{18}$$

and

$$R_2(x) = \begin{cases} g_1(x) := \alpha - s_x x & \text{if } x_M > x \geq 0 \\ g_2(x) := 0 & \text{if } x \geq x_M \end{cases} \tag{19}$$

where

$$\alpha = \frac{a}{2b_2}; \quad s_x = \frac{\gamma_2}{2b_2}; \quad x_M = \frac{a}{\gamma_2} \tag{20}$$

Then, the dynamics of the two-dimensional map $T(x, y) = (R_1(y), R_2(x))$ can be studied via the one-dimensional (composite) map F:

$$F(x) = R_1 \circ R_2(x) \tag{21}$$

as detailed in Appendix A.

Concerning the analytical expression of F, note that for $x > x_M$, we have $R_2(x) = 0$. Then, $F(x) = R_1(0) = \mu_L$ for $x > x_M$. Instead, for $x < x_M$, we have $R_2(x) = g_1(x) := \alpha - s_x x$. It follows that $g_1(x) < y_L$ for $x > \eta_3$, with

$$\eta_3 = \frac{\alpha - y_L}{s_x} \left(= \frac{a}{\gamma_2} \left(1 - \frac{2b_2\left(\overline{b}_1 - \underline{b}_1\right)}{\underline{\gamma}_1\left(\overline{b}_1 - \underline{b}_1\right) + 2\overline{b}_1\left(\overline{\gamma}_1 - \underline{\gamma}_1\right)} \right) \right) \tag{22}$$

[10] Note that the worst-case approach to uncertainty can be relax by adopting, for example, the α maxmin model, due to Arrow and Hurwicz (1972).

moreover, it follows that $g_1(x) < y_U$ for $x > \eta_2$, with

$$\eta_2 = \frac{\alpha - y_U}{s_x} \left(= \frac{a}{\gamma_2} \left(1 - \frac{2b_2 \left(\overline{b}_1 - \underline{b}_1 \right)}{\overline{\gamma}_1 \left(\overline{b}_1 - \underline{b}_1 \right) + 2\underline{b}_1 \left(\overline{\gamma}_1 - \underline{\gamma}_1 \right)} \right) \right) \tag{23}$$

and, finally, it follows that $g_1(x) < y_M$ for $x > \eta_1$, with

$$\eta_1 = \frac{\alpha - y_M}{s_x} \left(= \frac{a}{\gamma_2} \left(1 - \frac{2b_2}{\overline{\gamma}_1} \right) \right) \tag{24}$$

Note that $\eta_1 < \eta_2 < \eta_3 < x_M$, $\eta_1 < 0$ for $\alpha < y_M$ $\left(\overline{\gamma}_1 < 2b_2 \right)$, $\eta_2 < 0$ for $\alpha < y_U$ $\left(2\underline{b}_1 r + \overline{\gamma}_1 < 2b_2 \right)$ and $\eta_3 < 0$ when $\alpha < y_L$ $\left(2\overline{b}_1 r + \underline{\gamma}_1 < 2b_2 \right)$. Thus, for $\eta_1 > 0$ we have

$$F(x) = \begin{cases} F_0(x) := 0 & \text{if} \quad \eta_1 > x \geq 0 \\ F_1(x) := \mu_U - s_U g_1(x) & \text{if} \quad \eta_2 > x \geq \eta_1 \\ F_2(x) := r g_1(x) & \text{if} \quad \eta_3 > x \geq \eta_2 \\ F_3(x) := \mu_L - s_L g_1(x) & \text{if} \quad x_M > x \geq \eta_3 \\ F_4(x) := \mu_L & \text{if} \quad x \geq x_M \end{cases} \tag{25}$$

Instead, for $\eta_1 < 0$ and $\eta_2 > 0$ we have

$$F(x) = \begin{cases} F_1(x) := \mu_U - s_U g_1(x) & \text{if } \eta_2 > x \geq 0 \\ F_2(x) := r g_1(x) & \text{if } \eta_3 > x \geq \eta_2 \\ F_3(x) := \mu_L - s_L g_1(x) & \text{if } x_M > x \geq \eta_3 \\ F_4(x) := \mu_L & \text{if } x \geq x_M \end{cases} \tag{26}$$

Moreover, for $\eta_2 < 0$ and $\eta_3 > 0$ we have

$$F(x) = \begin{cases} F_2(x) := r g_1(x) & \text{if} \quad \eta_3 > x \geq 0 \\ F_3(x) := \mu_L - s_L g_1(x) & \text{if} \quad x_M > x \geq \eta_3 \\ F_4(x) := \mu_L & \text{if} \quad x \geq x_M \end{cases} \tag{27}$$

Finally, for $\eta_3 < 0$ we have

$$F(x) = \begin{cases} F_3(x) := \mu_L - s_L g_1(x) & \text{if } x_M > x \geq 0 \\ F_4(x) := \mu_L & \text{if } x \geq x_M \end{cases} \tag{28}$$

The maps F and T depend on several parameters, one of which is $a > 0$. However, any variation of parameter $a > 0$ has only a scaling effect: for any $a > 0$ we have $F(x) = aF(x/a)$ and $T(x, y) = aT(x/a, y/a)$, so that putting $x := x/a$ and $y := y/a$ we get topologically conjugate maps. Therefore, a is a scaling parameter for F and T and is set equal to 1 in the following without loss of generality. Moreover, map F has other relevant features that allow us to study its dynamics and are stated in the following proposition.

Proposition 1 *The map F has the following properties:*

(a) *It is continuous: $F_0(\eta_1) = F_1(\eta_1) = 0$, $F_1(\eta_2) = F_2(\eta_2) = r y_U$, $F_2(\eta_3) = F_3(\eta_3) = r y_L$ and $F_3(x_M) = F_4(x_M) = \mu_L$.*
(b) $F_0' = 0$.
(c) $F_1' = s_U s_x > 0$ *and* $F_1' > 1$ *for* $s_x > \frac{1}{s_U}$.
(d) $F_2' = -r s_x < 0$ *and* $F_2' < -1$ *for* $s_x > \frac{1}{r}$.
(e) $F_3' = s_L s_x > 0$ *and* $F_3' < F_1'$.

(f) $F_4^{'} = 0$.
(f) $F(x) \geq 0$ *for all* $x \geq 0$.

Proof of Proposition 1 Function F is made of up to five branches, F_i, $i = 0, \ldots, 4$, and each branch is a linear (affine linear) function. Therefore, the points η_1, η_2, η_3 and x_M at which F changes definition are the only possible points of discontinuity. However, since (as it can be easily verified) $F_0(\eta_1) = F_1(\eta_1) = 0$, $F_1(\eta_2) = F_2(\eta_2) = rg_1(\eta_2) = ry_U$, $F_2(\eta_3) = F_3(\eta_3) = rg_1(\eta_3) = ry_L$ and $F_3(x_M) = F_4(x_M) = \mu_L$, we have that F is a continuous function. Computing the slopes (first derivatives) of F_i and noting that $s_U s_x = \frac{\overline{\gamma}_1\gamma_2}{4\underline{b}_1 b_2} > s_L s_x = \frac{\underline{\gamma}_1\gamma_2}{4b_2\overline{b}_1} > 0$, properties (b)–(f) follow. The last property follows by noting that F has at most two minimal points, that is 0 and η_3, and $F(\eta_3) \geq F(0) = 0$. □

Moreover, we have the following general results about equilibria and their local asymptotic stability for F, F_0, F_1, F_2, F_3 and F_4.

Proposition 2 *Map* F *can have from 1 to 5 coexisting fixed points:*

- *Function* F_0 *has the unique equilibrium* $x_0^* = 0$*, existing and being unique in* $[0, \eta_1)$ *for* F *when* $\eta_1 > 0$*. This equilibrium is super stable;*
- *Function* F_1 *has the unique equilibrium* $x_1^* = \frac{2b_2 - \overline{\gamma}_1}{4\underline{b}_1 b_2 - \overline{\gamma}_1\gamma_2}$*, which is locally-asymptotically stable for* $\frac{\overline{\gamma}_1\gamma_2}{4\underline{b}_1 b_2} < 1$*. This equilibrium exists also for* F *when* $\eta_2 > 0$ *and* $\max\{\eta_1; 0\} < x_1^* < \eta_2$ *(equivalently when either* $\eta_1 < 0 < F(\eta_2) < \eta_2$ *or* $F(\eta_2) > \eta_2 > \eta_1 > 0$*) and is unstable for* $\eta_1 > 0$ *and locally-asymptotically stable otherwise;*
- *Function* F_2 *has the unique equilibrium* $x_2^* = \frac{r}{2b_2 + r\gamma_2}$*, existing for* F *when* $\eta_3 > 0$ *and* $\max\{\eta_2; 0\} < x_2^* < \eta_3$ *(equivalently when* $F(\eta_3) < \eta_3$ *and either* $\eta_2 < 0 < \eta_3$ *or* $F(\eta_2) > \eta_2 > 0$*). This equilibrium is locally-asymptotically stable for* $r\frac{\gamma_2}{2\overline{b}_2} < 1$*;*
- *Function* F_3 *has the unique equilibrium* $x_3^* = \frac{2b_2 - \underline{\gamma}_1}{4\overline{b}_1 b_2 - \underline{\gamma}_1\gamma_2}$*, which is locally-asymptotically stable for* $\frac{\underline{\gamma}_1\gamma_2}{4\overline{b}_1 b_2} < 1$*. This equilibrium exists also for* F *when* $\max\{\eta_3, 0\} < x_3^* < x_M$*. Specifically, it is locally-asymptotically stable for* $F(\max\{\eta_3, 0\}) > \max\{\eta_3, 0\}$ *and* $F(x_M) < x_M$*, while it is unstable for* $F(\max\{\eta_3, 0\}) < \max\{\eta_3, 0\}$ *and* $F(x_M) > x_M$*.*
- *Function* F_4 *has the unique equilibrium* $x_4^* = \frac{1}{2\overline{b}_1}$ $(= \mu_L)$*, existing and being unique in* $(x_M, +\infty)$ *for* F *when* $x_M < x_4^* = F(x_M)$*. This equilibrium is super stable;*

Proof of Properties 2 For all $i \in \{0, \ldots, 4\}$, the function F_i is either linear and constant or affine linear. Therefore, each function F_i has at most one isolated equilibrium that solves $F_i(x) = x$ and which is locally-asymptotically stable if and only if the slope of F_i is in absolute value smaller than one. This completes the proof. □

The properties of map F, as stated in Propositions 1 and 2, can be used to prove the following results about existence and stability of Cournot–Nash equilibria. These results are with regards to the entire parameter space identified by Assumption 1. Note that this parameter space includes also realizations where $\gamma_1 > b_2$ and $\gamma_2 > b_1$. Specifically, the conditions $\overline{\gamma}_1 > 2b_2$, $\underline{\gamma}_1 > 2b_2$, $\gamma_2 > 2\underline{b}_1$, $\gamma_2 > 2\overline{b}_1$, that appear in the following proposition, can be interpreted as pessimistic beliefs of firm 1, resp. firm 2, on the sensitivity of the market price of its products with respect to the level of production of the competitor.

Proposition 3 *Consider the equilibria* x_0^**,* x_1^**,* x_2^**,* x_3^* *and* x_4^* *defined in Proposition 1 and consider map* F*, we have the following possible cases:*

1. *If* $\eta_1 > 0$ *(*$\overline{\gamma}_1 > 2b_2$*),* $F(\eta_2) < \eta_2$ *(*$\left(\overline{\gamma}_1 - 2b_2\right) > r\left(\gamma_2 - 2\underline{b}_1\right)$*) and* $F(x_M) < x_M$ *(*$\gamma_2 < 2\overline{b}_1$*), then* x_0^* *is the unique equilibrium and is globally attracting;*
2. *If* $\eta_1 > 0$ *(*$\overline{\gamma}_1 > 2b_2$*),* $F(\eta_2) < \eta_2$ *(*$\left(\overline{\gamma}_1 - 2b_2\right) > r\left(\gamma_2 - 2\underline{b}_1\right)$*) and* $F(x_M) > x_M$ *(*$\gamma_2 > 2\overline{b}_1$*), then* x_0^**,* x_3^* *and* x_4^* *are the only equilibria,* x_0^* *and* x_4^* *are locally-asymptotically stable while* x_3^* *is unstable and* $\mathcal{B}\left(x_0^*\right) = \left[0, x_3^*\right)$ *and* $\mathcal{B}\left(x_4^*\right) = \left(x_3^*, +\infty\right)$*;*
3. *If* $\eta_1 > 0$ *(*$\overline{\gamma}_1 > 2b_2$*),* $F(\eta_2) > \eta_2$ *(*$\left(\overline{\gamma}_1 - 2b_2\right) < r\left(\gamma_2 - 2\underline{b}_1\right)$*),* $F(\eta_3) > \eta_3$ *(*$r\left(\gamma_2 - 2\overline{b}_1\right) > \underline{\gamma}_1 - 2b_2$*), and* $F(x_M) < x_M$ *(*$\gamma_2 < 2\overline{b}_1$*), then* x_0^**,* x_1^* *and* x_3^* *are the only equilibria,* x_0^* *and* x_3^* *are locally-asymptotically stable with basins of attraction given by* $\mathcal{B}\left(x_0^*\right) = \left[0, x_1^*\right)$ *and* $\mathcal{B}\left(x_3^*\right) = \left(x_1^*, +\infty\right)$*, respectively, while* x_1^* *is unstable.*
4. *If* $\eta_1 > 0$ *(*$\overline{\gamma}_1 > 2b_2$*),* $F(\eta_2) > \eta_2$ *(*$\left(\overline{\gamma}_1 - 2b_2\right) < r\left(\gamma_2 - 2\underline{b}_1\right)$*),* $F(\eta_3) > \eta_3$ *(*$r\left(\gamma_2 - 2\overline{b}_1\right) > \underline{\gamma}_1 - 2b_2$*), and* $F(x_M) > x_M$ *(*$\gamma_2 > 2\overline{b}_1$*), then* x_0^**,* x_1^* *and* x_4^* *are the only equilibria,* x_0^* *and* x_4^* *are locally-asymptotically stable with basins of attraction given by* $\mathcal{B}\left(x_0^*\right) = \left[0, x_1^*\right)$ *and* $\mathcal{B}\left(x_4^*\right) = \left(x_1^*, +\infty\right)$*, respectively, while* x_1^* *is unstable;*
5. *If* $\eta_1 > 0$ *(*$\overline{\gamma}_1 > 2b_2$*),* $F(\eta_2) > \eta_2$ *(*$\left(\overline{\gamma}_1 - 2b_2\right) < r\left(\gamma_2 - 2\underline{b}_1\right)$*),* $F(\eta_3) < \eta_3$ *(*$r\left(\gamma_2 - 2\overline{b}_1\right) < \underline{\gamma}_1 - 2b_2$*), and* $F(x_M) > x_M$ *(*$\gamma_2 > 2\overline{b}_1$*), then* x_0^**,* x_1^**,* x_2^**,* x_3^* *and* x_4^* *are the only equilibria,* x_0^* *and* x_4^* *are super stable,* x_1^* *and* x_3^* *are unstable, while*

   (i) x_2^* *is locally-asymptotically stable,* $\mathcal{B}\left(x_0^*\right) \supseteq \left[0, x_1^*\right)$*,* $\mathcal{B}\left(x_2^*\right) \subseteq \left(x_1^*, x_3^*\right)$ *and* $\mathcal{B}\left(x_4^*\right) \supseteq \left(x_3^*, +\infty\right)$ *for* $r\gamma_2 < 2b_2$*. Moreover,* $\mathcal{B}\left(x_0^*\right) = \left[0, x_1^*\right)$*,* $\mathcal{B}\left(x_2^*\right) = \left(x_1^*, x_3^*\right)$ *and* $\mathcal{B}\left(x_4^*\right) = \left(x_3^*, +\infty\right)$ *when*

$$2b_2\left(\frac{\left(\overline{\gamma}_1 - 2b_2\right)\left(\underline{\gamma}_1 + 2\overline{b}_1 r\right)}{\overline{\gamma}_1\left(\underline{\gamma}_1 + 2\overline{b}_1 r - 2b_2\right)} + \frac{2\underline{b}_1}{\overline{\gamma}_1} r\right) < r\gamma_2$$
$$< 2b_2 \min\left\{1, \left(\frac{\left(\overline{\gamma}_1 + 2\underline{b}_1 r\right)\left(\underline{\gamma}_1 - 2b_2\right)}{\underline{\gamma}_1\left(\overline{\gamma}_1 + 2\underline{b}_1 r - 2b_2\right)} + \frac{2\overline{b}_1}{\underline{\gamma}_1} r\right)\right\}; \tag{29}$$

   (ii) x_2^* *is unstable,* $\mathcal{B}\left(x_1^*\right) \supseteq \left[0, x_1^*\right)$*,* $\mathcal{B}\left(x_4^*\right) \supseteq \left(x_3^*, +\infty\right)$ *(an attracting cycles, or a chaotic attractor, or a chaotic repellor may exist) for* $r\gamma_2 > 2b_2$*;*

6. *If* $\eta_1 > 0$ *(*$\overline{\gamma}_1 > 2b_2$*),* $F(\eta_2) > \eta_2$ *(*$\left(\overline{\gamma}_1 - 2b_2\right) < r\left(\gamma_2 - 2\underline{b}_1\right)$*),* $F(\eta_3) < \eta_3$ *(*$r\left(\gamma_2 - 2\overline{b}_1\right) < \underline{\gamma}_1 - 2b_2$*), and* $F(x_M) < x_M$ *(*$\gamma_2 < 2\overline{b}_1$*), then* x_0^**,* x_1^* *and* x_2^* *are the only equilibria,* x_0^* *is super stable,* x_1^* *is unstable, while*

   (i) x_2^* *is locally-asymptotically stable,* $\mathcal{B}\left(x_1^*\right) \supseteq \left[0, x_1^*\right)$ *and* $\mathcal{B}\left(x_2^*\right) \subseteq \left(x_1^*, +\infty\right)$ *for* $r\gamma_2 < 2b_2$*. Moreover,* $\mathcal{B}\left(x_1^*\right) = \left[0, x_1^*\right)$ *and* $\mathcal{B}\left(x_2^*\right) = \left(x_1^*, +\infty\right)$ *when*

$$2b_2\left(\frac{\left(\overline{\gamma}_1 - 2b_2\right)\left(\underline{\gamma}_1 + 2\overline{b}_1 r\right)}{\overline{\gamma}_1\left(\underline{\gamma}_1 + 2\overline{b}_1 r - 2b_2\right)} + \frac{2\underline{b}_1}{\overline{\gamma}_1} r\right) < r\gamma_2 < 2b_2; \tag{30}$$

   (ii) x_2^* *is unstable,* $\mathcal{B}\left(x_1^*\right) \supseteq \left[0, x_1^*\right)$ *(an attracting cycles, or a chaotic attractor, or a chaotic repellor may exist) for* $r\gamma_2 > 2b_2$*;*

7. *If* $\eta_1 < 0$ *(*$\overline{\gamma}_1 < 2b_2$*) and* $\eta_2 > 0$ *(*$2b_2 < \left(2\underline{b}_1 r + \overline{\gamma}_1\right)$*),* $F(\eta_2) < \eta_2$ *(*$\left(\overline{\gamma}_1 - 2b_2\right) > r\left(\gamma_2 - 2\underline{b}_1\right)$*) and* $F(x_M) < x_M$ *(*$\gamma_2 < 2\overline{b}_1$*), then* x_1^* *is the unique equilibrium and is globally attracting;*

8. *If* $\eta_1 < 0$ ($\overline{\gamma}_1 < 2b_2$) *and* $\eta_2 > 0$ ($2b_2 < \left(2\underline{b}_1 r + \overline{\gamma}_1\right)$), $F(\eta_2) > \eta_2$ ($\left(\overline{\gamma}_1 - 2b_2\right) < r\left(\gamma_2 - 2\underline{b}_1\right)$), $F(\eta_3) > \eta_3$ ($r\left(\gamma_2 - 2\overline{b}_1\right) > \underline{\gamma}_1 - 2b_2$), *and* $F(x_M) < x_M$ ($\gamma_2 < 2\overline{b}_1$), *then* x_3^* *is the unique equilibrium and is globally attracting;*
9. *If* $\eta_1 < 0$ ($\overline{\gamma}_1 < 2b_2$) *and* $\eta_2 > 0$ ($2b_2 < \left(2\underline{b}_1 r + \overline{\gamma}_1\right)$), $F(\eta_2) > \eta_2$ ($\left(\overline{\gamma}_1 - 2b_2\right) < r\left(\gamma_2 - 2\underline{b}_1\right)$), $F(\eta_3) > \eta_3$ ($r\left(\gamma_2 - 2\overline{b}_1\right) > \underline{\gamma}_1 - 2b_2$), *and* $F(x_M) > x_M$ ($\gamma_2 > 2\overline{b}_1$), *then* x_4^* *is the unique equilibrium and is globally attracting;*
10. *If* $\eta_1 < 0$ ($\overline{\gamma}_1 < 2b_2$) *and* $\eta_2 > 0$ ($2b_2 < \left(2\underline{b}_1 r + \overline{\gamma}_1\right)$), $F(\eta_2) > \eta_2$ ($\left(\overline{\gamma}_1 - 2b_2\right) < r\left(\gamma_2 - 2\underline{b}_1\right)$), $F(\eta_3) < \eta_3$ ($r\left(\gamma_2 - 2\overline{b}_1\right) < \underline{\gamma}_1 - 2b_2$), *and* $F(x_M) < x_M$ ($\gamma_2 < 2\overline{b}_1$), *then* x_2^* *is the unique equilibrium and it is*

    (i) *globally attracting for* $r\gamma_2 < 2b_2$;
    (ii) *unstable for* $r\gamma_2 > 2b_2$ *and a unique attracting set exists which is globally attracting (expect for* x_2^**). It belongs to* $\left[F(\eta_3), F^2(\eta_3)\right]$ *when* η_3 *is closer to* x_2^* *than* η_2 *and it belongs to* $\left[F(\eta_2), F^2(\eta_2)\right]$ *otherwise.*

11. *If* $\eta_1 < 0$ ($\overline{\gamma}_1 < 2b_2$) *and* $\eta_2 < 0$ ($2b_2 > \left(2\underline{b}_1 r + \overline{\gamma}_1\right)$), $\eta_3 > 0$ ($2b_2 < 2\overline{b}_1 r + \underline{\gamma}_1$), $F(\eta_3) > \eta_3$ ($r\left(\gamma_2 - 2\overline{b}_1\right) > \underline{\gamma}_1 - 2b_2$) *and* $F(x_M) < x_M$ ($\gamma_2 < 2\overline{b}_1$), *then* x_3^* *is the unique equilibrium and is globally attracting;*
12. *If* $\eta_1 < 0$ ($\overline{\gamma}_1 < 2b_2$) *and* $\eta_2 < 0$ ($2b_2 > \left(2\underline{b}_1 r + \overline{\gamma}_1\right)$), $\eta_3 > 0$ ($2b_2 < 2\overline{b}_1 r + \underline{\gamma}_1$), $F(\eta_3) > \eta_3$ ($r\left(\gamma_2 - 2\overline{b}_1\right) > \underline{\gamma}_1 - 2b_2$) *and* $F(x_M) > x_M$ ($\gamma_2 > 2\overline{b}_1$), *then* x_4^* *is the unique equilibrium and is globally attracting.*
13. *If* $\eta_1 < 0$ ($\overline{\gamma}_1 < 2b_2$) *and* $\eta_2 < 0$ ($2b_2 > \left(2\underline{b}_1 r + \overline{\gamma}_1\right)$), $\eta_3 > 0$ ($2b_2 < 2\overline{b}_1 r + \underline{\gamma}_1$), $F(\eta_3) < \eta_3$ ($r\left(\gamma_2 - 2\overline{b}_1\right) < \underline{\gamma}_1 - 2b_2$) *and* $F(x_M) < x_M$ ($\gamma_2 < 2\overline{b}_1$), *then* x_2^* *is the unique equilibrium and is globally attracting.*
14. *If* $\eta_1 < 0$ ($\overline{\gamma}_1 < 2b_2$) *and* $\eta_2 < 0$ ($2b_2 > \left(2\underline{b}_1 r + \overline{\gamma}_1\right)$), $\eta_3 < 0$ ($2b_2 > 2\overline{b}_1 r + \underline{\gamma}_1$), $F(x_M) < x_M$ ($\gamma_2 < 2\overline{b}_1$), *then* x_3^* *is the unique equilibrium and is globally attracting;*
15. *If* $\eta_1 < 0$ ($\overline{\gamma}_1 < 2b_2$) *and* $\eta_2 < 0$ ($2b_2 > \left(2\underline{b}_1 r + \overline{\gamma}_1\right)$), $\eta_3 < 0$ ($2b_2 > 2\overline{b}_1 r + \underline{\gamma}_1$), $F(x_M) > x_M$ ($\gamma_2 > 2\overline{b}_1$), *then* x_4^* *is the unique equilibrium and is globally attracting.*

No other configurations are possible.

Proof of Proposition 3 By definition $\eta_1 < \eta_2 < \eta_3 < x_M$, $x_M > 0$, and the piecewise linear map F is continuous as stated in Proposition 1, has five branches when $\eta_1 > 0$, four branches when $\eta_1 < 0$ and $\eta_2 > 0$, three branches when $\eta_2 < 0$ and $\eta_3 > 0$, and two branches when $\eta_3 < 0$.

Consider $\eta_1 > 0$. It follows that F is constant and equal to zero in $[0, \eta_1]$, strictly increasing in $[\eta_1, \eta_2]$, strictly decreasing in $[\eta_2, \eta_3]$, increasing in $[\eta_3, x_M]$ and constant for $x > x_M$. Then $F(\eta_2) < \eta_2$ implies $F(\eta_3) < \eta_3$ and there are 6 (instead of 8) possible combinations of $F(\eta_2) \lessgtr \eta_2$, $F(\eta_3) \lessgtr \eta_3$ and $F(x_M) \lessgtr x_M$: Case 1 ($F(\eta_2) < \eta_2$ and $F(x_M) < x_M$), Case 2 ($F(\eta_2) < \eta_2$ and $F(x_M) > x_M$), Case 3 ($F(\eta_2) > \eta_2$, $F(\eta_3) > \eta_3$ and $F(x_M) < x_M$), Case 4 ($F(\eta_2) > \eta_2$, $F(\eta_3) > \eta_3$ and $F(x_M) > x_M$), Case 5 ($F(\eta_2) > \eta_2$, $F(\eta_3) < \eta_3$ and $F(x_M) > x_M$), Case 6 ($F(\eta_2) > \eta_2$, $F(\eta_3) < \eta_3$ and $F(x_M) < x_M$). The properties (continuity) of F in Proposition 1 and the conditions that define Case 1 imply that x_0^* (superstable) is the unique equilibrium of F (see Proposition 2) and $F(x) < x$ for all $x > 0$. Therefore, x_0^* is globally attracting. The properties (continuity) of F in Proposition 1 and the conditions that define Case 2 imply that x_0^* (superstable), x_3^* (unstable) and x_4^* (superstable) are the equilibria of F (see Proposition 2), $F(x) < x$ for all $x < x_3^*$ and $F(x) > x$ for all $x \in \left(x_3^*, x_4^*\right)$. Therefore, each point of $\left[0, x_3^*\right)$ is mapped in a few iterations into $x_0^* = 0$, each point of $\left(x_3^*, x_4^*\right)$ is mapped in $x \geq x_4^*$ in a few

iterations, each point in $\left(x_4^*, \infty\right)$ is mapped in x_4^* in a single iteration and we can conclude that $\mathcal{B}\left(x_0^*\right) = \left[0, x_3^*\right)$ and $\mathcal{B}\left(x_4^*\right) = \left(x_3^*, +\infty\right)$. The properties (continuity) of F in Proposition 1 and the conditions that define Case 3 imply that x_0^* (superstable), x_1^* (unstable) and x_3^* (locally-asymptotically stable) are the only equilibria of F (see Proposition 2), $x > F(x)$ for all $x \in \left(0, x_1^*\right)$, $x < F(x)$ for all $x \in \left(x_1^*, \eta_3\right)$ (then all points in $\left(x_1^*, \eta_3\right)$ are mapped in $x > x_3^*$ in a few iterations), all points in $[x_M, \infty)$ are mapped in a single iteration in $\mu_L \in (\eta_3, x_M)$, and all points in (η_3, x_M) converges monotonically to x_3^* (because F is there linear with a slope that is positive but smaller than 1). Therefore, $\mathcal{B}\left(x_0^*\right) = \left[0, x_1^*\right)$ and $\mathcal{B}\left(x_3^*\right) = \left(x_1^*, +\infty\right)$. The properties (continuity) of F in Proposition 1 and the conditions that define Case 4 imply x_0^* (superstable), x_1^* (unstable) and x_4^* (superstable) are the equilibria of F (see Proposition 2), $x > F(x)$ for all $x \in \left(0, x_1^*\right)$, $x < F(x)$ for all $x \in \left(x_1^*, x_M\right)$ (then all points in $\left(x_1^*, x_M\right)$ are mapped into $x \geq x_M$ in a few iterations) and each point in $[x_M, \infty)$ is mapped in x_4^* in at most one iteration. Therefore, $\mathcal{B}\left(x_0^*\right) = \left[0, x_1^*\right)$ and $\mathcal{B}\left(x_4^*\right) = \left(x_1^*, +\infty\right)$. The properties (continuity) of F in Proposition 1 and the conditions that define Case 5(i) imply that x_0^* (superstable), x_1^* (unstable), x_2^* (locally-asymptotically stable), x_3^* (unstable), and x_4^* (superstable) are the equilibria of F (see Proposition 2), $x > F(x)$ for all $x \in \left(0, x_1^*\right)$, $x < F(x)$ for all $x \in \left(x_3^*, x_M\right)$ (then each point in $\left(x_3^*, x_M\right)$ is mapped in $x > x_M$ in a few iterations) and each point in $[x_M, \infty)$ is mapped in x_4^* in at most one iteration. Therefore, $\mathcal{B}\left(x_0^*\right) \supseteq \left[0, x_1^*\right)$, $\mathcal{B}\left(x_2^*\right) \subseteq \left(x_1^*, x_3^*\right)$ and $\mathcal{B}\left(x_4^*\right) \supseteq \left(x_3^*, +\infty\right)$. Further imposing $F(\eta_2) < x_3^*$ and $F(\eta_3) > x_1^*$, we have that $x_1^* < F(x) < x_3^*$ for all $x \in \left(x_1^*, x_3^*\right)$. Therefore, $\left(x_1^*, x_3^*\right)$ is a trapping set. Moreover, if $\left|\eta_2 - x_2^*\right| > \left|\eta_3 - x_2^*\right|$, then $F(\eta_3) \in (\eta_2, \eta_3)$ and we have that $[F(\eta_3), \eta_3]$ is an absorbing invariant set. Inside this invariant set F is decreasing-increasing with slope of the decreasing branch that is higher than -1. Therefore, the map is conjugate to the skew-tent map, see Sushko et al. (2016) and Avrutin et al. (2019), from which we know that x_2^* attracts all points in the invariant set. On the contrary, if $\left|\eta_2 - x_2^*\right| < \left|\eta_3 - x_2^*\right|$, then $F(\eta_2) \in (\eta_2, \eta_3)$ and we have that $[\eta_2, F(\eta_2)]$ is an absorbing invariant set. Inside this invariant set F is increasing-decreasing with slope of the decreasing branch that is higher than -1. Therefore, the map is conjugate to the skew-tent map, see Sushko et al. (2016) and Avrutin et al. (2019), from which we know that x_2^* attracts again all points in the invariant set. Thus, $\mathcal{B}\left(x_0^*\right) = \left[0, x_1^*\right)$, $\mathcal{B}\left(x_2^*\right) = \left(x_1^*, x_3^*\right)$ and $\mathcal{B}\left(x_4^*\right) = \left(x_3^*, +\infty\right)$. Note that $\overline{\gamma}_1 > \underline{\gamma}_1 > 2b_2$ in Case 5, $4\underline{b}_1 b_2 - \overline{\gamma}_1\gamma_2 < 0$ since $x_1^* > 0$ and $4\overline{b}_1 b_2 < \underline{\gamma}_1\gamma_2$ in order to have $x_3^* > 0$. Therefore,

$$
\begin{aligned}
F(\eta_3) > x_1^* \Leftrightarrow\ & r\left(\frac{\underline{\gamma}_1 + 2\overline{b}_1 r - 2b_2}{2b_2\left(\underline{\gamma}_1 + 2\overline{b}_1 r\right)}\right) > \frac{2b_2 - \overline{\gamma}_1}{4\underline{b}_1 b_2 - \overline{\gamma}_1\gamma_2} \\
\Leftrightarrow\ & 2b_2\left(\frac{\left(\overline{\gamma}_1 - 2b_2\right)\left(\underline{\gamma}_1 + 2\overline{b}_1 r\right)}{r\overline{\gamma}_1\left(\underline{\gamma}_1 + 2\overline{b}_1 r - 2b_2\right)} + \frac{2\underline{b}_1}{\overline{\gamma}_1}\right) < \gamma_2
\end{aligned} \tag{31}
$$

and

$$
\begin{aligned}
F(\eta_2) < x_3^* \Leftrightarrow\ & r\frac{\overline{\gamma}_1 + 2\underline{b}_1 r - 2b_2}{2b_2\left(\overline{\gamma}_1 + 2\underline{b}_1 r\right)} < \frac{2b_2 - \underline{\gamma}_1}{4\overline{b}_1 b_2 - \underline{\gamma}_1\gamma_2} \\
\Leftrightarrow\ & 2b_2\left(\frac{\left(\overline{\gamma}_1 + 2\underline{b}_1 r\right)\left(\underline{\gamma}_1 - 2b_2\right)}{r\underline{\gamma}_1\left(\overline{\gamma}_1 + 2\underline{b}_1 r - 2b_2\right)} + \frac{2\overline{b}_1}{\underline{\gamma}_1}\right) > \gamma_2
\end{aligned} \tag{32}
$$

Case 5(ii) is as Case 5(i) but x_2^* is unstable because $2b_2 > r\gamma_2$ implies a slope of F in $[\eta_2, \eta_3]$ which is smaller than -1 and $\mathcal{B}\left(x_0^*\right) \supseteq \left[0, x_1^*\right)$ and $\mathcal{B}\left(x_4^*\right) \supseteq \left(x_3^*, +\infty\right)$. The existence of an attracting cycle, chaotic attractor or chaotic repellor follows by employing the skew tent map as a border collision normal form (BCNF), see Sushko et al. (2016) and Avrutin et al. (2019)). The properties (continuity) of F in Proposition 1 and the conditions that define Case 6(i) imply that x_0^* (superstable), x_1^* (unstable) and x_2^* (locally-asymptotically stable) are the only equilibria of F (see Proposition 2), $x > F(x)$ for all $x \in \left(0, x_1^*\right)$. Therefore, $\mathcal{B}\left(x_0^*\right) \supseteq \left[0, x_1^*\right)$. Moreover, η_3 is the unique local minimum point of F in $\left(x_1^*, +\infty\right)$. Then, $F(\eta_3) > x_1^*$ implies that $\left(x_1^*, +\infty\right)$ is an invariant set. Since there cannot be other attractors in $\left(x_1^*, +\infty\right)$ than x_2^* as it follows by using the skew-tent map as a border collision normal form, see Sushko et al. (2016) and Avrutin et al. (2019), we have that $\mathcal{B}\left(x_0^*\right) = \left[0, x_1^*\right)$ and $\mathcal{B}\left(x_2^*\right) = \left(x_1^*, +\infty\right)$. Case 6(ii) is as Case 6(i) but the slope of F in (η_2, η_3) is smaller than -1. Therefore, x_2^* is unstable (see Proposition 2). Then, assuming that $\left(x_1^*, +\infty\right)$ is invariant, we have that either $[\eta_2, F(\eta_2)]$ (if $\left|\eta_2 - x_2^*\right| < \left|\eta_3 - x_2^*\right|$) or $[F(\eta_3), \eta_3]$ (if $\left|\eta_2 - x_2^*\right| > \left|\eta_3 - x_2^*\right|$) is an absorbing interval where the map is conjugate to the skew-tent map and we are in the case where the decreasing branch has a slope smaller than -1 and the second higher than 1. This allows us to conclude that there could be a cycle with periodicity related to the main tongues, that is, 2 or 3 or 4 and so on, alternatively we can have 2^m cyclical chaotic attractors with m a positive integer number. Specifically, the result of the degenerate flip bifurcation at which undergoes x_2^* when the associated eigenvalue crosses the value -1 may be determined by using the skew tent map as a border collision normal form (BCNF), see Sushko et al. (2016) and Avrutin et al. (2019).

Consider $\eta_1 < 0$ and $\eta_2 > 0$. It follows that $0 < \eta_2 < \eta_3 < x_M$ with the piecewise linear map F that is strictly increasing in $[0, \eta_2]$, strictly decreasing in $[\eta_2, \eta_3]$, increasing in $[\eta_3, x_M]$ and constant for $x > x_M$. Then, $F(\eta_2) < \eta_2$ implies $F(\eta_3) < \eta_3$ and there are 6 (instead of 8) possible combinations of $F(\eta_2) \lesseqgtr \eta_2$, $F(\eta_3) \lesseqgtr \eta_3$ and $F(x_M) \lesseqgtr x_M$: Case 7 ($F(\eta_2) < \eta_2$ and $F(x_M) < x_M$), Case N1 ($F(\eta_2) < \eta_2$ and $F(x_M) > x_M$), Case 8 ($F(\eta_2) > \eta_2$, $F(\eta_3) > \eta_3$ and $F(x_M) < x_M$), Case 9 ($F(\eta_2) > \eta_2$, $F(\eta_3) > \eta_3$ and $F(x_M) > x_M$), Case 10 ($F(\eta_2) > \eta_2$, $F(\eta_3) < \eta_3$ and $F(x_M) < x_M$), Case N2 ($F(\eta_2) > \eta_2$, $F(\eta_3) < \eta_3$ and $F(x_M) > x_M$). Case N1 requires $\eta_1 < 0$ ($\overline{\gamma}_1 < 2b_2$), $F(\eta_2) < \eta_2$ ($\left(\overline{\gamma}_1 - 2b_2\right) > r\left(\gamma_2 - 2\underline{b}_1\right)$) and $F_3(x_M) = F_4(x_M) > x_M$ ($\gamma_2 > 2\overline{b}_1$). Since $\overline{b}_1 > \underline{b}_1$ by assumption, the first two conditions imply $\gamma_2 < 2\underline{b}_1$. This excludes the last condition to have Case N1 which is therefore not possible. Case N2 requires $\eta_1 < 0$ ($\overline{\gamma}_1 < 2b_2$), $F_2(\eta_3) = F_3(\eta_3) < \eta_3$ ($r\left(\gamma_2 - 2\overline{b}_1\right) < \underline{\gamma}_1 - 2b_2$), and $F_3(x_M) = F_4(x_M) > x_M$ ($\gamma_2 > 2\overline{b}_1$). Since $\overline{\gamma}_1 > \underline{\gamma}_1$ by assumption, the first two conditions imply $\gamma_2 < 2\overline{b}_1$. This contradicts the last condition to have Case N2 which is therefore impossible. The properties (continuity) of F in Proposition 1 and the conditions that define Case 7 imply that x_1^* (locally-asymptotically stable) is the only equilibrium of F (see Proposition 2), $F(x) < x$ for all $x > \eta_2$ and the slope of F in $[0, \eta_2]$ is positive but smaller than one. Then all points outside $[0, \eta_2]$ are mapped inside in a few iterations, and each point inside $[0, \eta_2]$ converges to x_1^* which is therefore globally attracting. The properties (continuity) of F in Proposition 1 and the conditions that define Case 8 imply that x_3^* (locally-asymptotically stable) is the only equilibrium of F (see Proposition 2), the slope of F is positive but smaller than one in (η_3, x_M) (then x_3^* attracts all points in (η_3, x_M)), $F(x) > x$ for all $x < \eta_3$ (then all points outside $[\eta_3, \infty)$ are mapped inside in a few iterations), all points in $[x_M, \infty)$ are mapped in μ_L in a single iteration and $\mu_L \in (\eta_3, x_M)$. This proves that x_3^* is globally attracting. The properties (continuity) of F in Proposition 1 and the conditions that define Case 9 imply that x_4^* (superstable) is the only equilibrium of F (see Proposition 2) and $F(x) > x$ for all $x < x_M$

(then all points outside $[x_M, \infty)$ are mapped inside in a few iterations). Since each point in $[x_M, \infty)$ is mapped into x_4^* in a single iteration by definition of F, we have that x_4^* is globally attracting. The properties (continuity) of F in Proposition 1 and the conditions that define Case 10 imply that x_2^* is the unique equilibrium of F (see Proposition 2), is locally-asymptotically stable when the slope of F in (η_2, η_3) is between -1 and 0, Case 10(i). It is unstable when the slope of F in (η_2, η_3) is smaller than -1, Case 10(ii). In Case 10(i), x_2^* is globally attracting since all points are mapped in a few iterations into the absorbing interval $\left[F(\eta_3), F^2(\eta_3)\right]$ where $F(\eta_3) = F_2(\eta_3) < \eta_3$ and $F^2(\eta_3)$ is either equal to $F_2 \circ F_2(\eta_3) < \eta_3$ (as F_2 is linear and contracting) or equal to $F_1 \circ F_2(\eta_3) < F_2 \circ F_2(\eta_3) < \eta_3$. In the first case, the absorbing interval is also invariant and inside this interval F is topologically conjugate to F_2. Therefore, all points are mapped into x_2^* in a few iterations. In the second case, the system is in $\left[F(\eta_3), F^2(\eta_3)\right]$ is topological conjugate to the skew tent map, that works as a border collision normal form (BCNF), see Sushko et al. (2016) and Avrutin et al. (2019), and from which it follows that all points are mapped into x_2^* in a few iterations. In Case 10(ii), consider $M_F = \max\{F(x_M), F(\eta_2)\}$ and $m_F = \min\{F(0), F(\eta_3)\}$ and by definition of F we have that m_F is the minimum of F and M_F is the maximum of F, that is $F(x) \in [m_F, M_F]$ for all $x \geq 0$. Therefore, $[m_F, M_F]$ is a trapping set for F and if the only equilibrium x_2^* that is inside this region is unstable, in this region there should be either a periodic or chaotic attractor. This invariant set is unique and is globally attracting by the skew-tent map, see Sushko et al. (2016) and Avrutin et al. (2019).

Consider $\eta_2 < 0$ and $\eta_3 > 0$. It follows that $0 < \eta_3 < x_M$ with the piecewise linear map F that is decreasing in $[0, \eta_3]$, increasing in $[\eta_3, x_M]$, and constant for $x > x_M$. Then, there are 4 possible combinations of $F(\eta_3) \lesseqgtr \eta_3$ and $F(x_M) \lesseqgtr x_M$: Case 11 ($F(\eta_3) > \eta_3$ and $F(x_M) < x_M$), Case 12 ($F(\eta_3) > \eta_3$ and $F(x_M) > x_M$), Case 13 ($F(\eta_3) < \eta_3$ and $F(x_M) < x_M$), Case N3 ($F(\eta_3) < \eta_3$ and $F(x_M) > x_M$). Case N3 requires the slope of F in (η_3, x_M) greater than 1 ($\underline{\gamma}_1\gamma_2 > 2\overline{b}_1 2b_2$), $F_3(x_M) = F_4(x_M) > x_M$ $\left(2\overline{b}_1 > \gamma_2\right)$ and $\eta_2 < 0$ $\left(2\underline{b}_1 r + \overline{\gamma}_1 < 2b_2\right)$. Since $2\underline{b}_1 r > 0$ and $\overline{\gamma}_1 > \underline{\gamma}_1$ by assumption, combining these three conditions we obtain the contradiction $\underline{\gamma}_1 > 2\underline{b}_1 r + \overline{\gamma}_1 > \underline{\gamma}_1$. Therefore, Case N3 is impossible. The properties (continuity) of F in Proposition 1 and the conditions that define Case 11 imply that x_3^* is the only equilibrium of F and is locally-asymptotically stable (see Proposition 2), $F(x) > x$ for all $x \in [0, \eta_3)$ (then all points outside $[\eta_3, +\infty)$ are mapped inside in a few iterations), all points in $(x_M, +\infty)$ are mapped in $\mu_L \in \left(x_3^*, x_M\right]$ in a single iteration, and the slope of F is positive but smaller than one in $[\eta_3, x_M]$ (then all points in $[\eta_3, x_M]$ converges to x_3^* in a few iterations). It follows that x_3^* is globally attracting. The properties (continuity) of F in Proposition 1 and the conditions that define Case 12 imply that x_4^* (superstable) is the only equilibrium of F (see Proposition 2), and $F(x) > x$ for all $x < x_M$. Therefore, each point outside $[x_M, \infty)$ is mapped inside into a few iterations and each point in $[x_M, \infty)$ is mapped into x_4^* in a single iteration. It follows that x_4^* is globally attracting. The properties (continuity) of F in Proposition 1 and the conditions that define Case 13 imply that x_2^* is the unique equilibrium of F and is locally-asymptotically stable for $r\gamma_2 < 2b_2$ and unstable for $r\gamma_2 > 2b_2$ (see Proposition 2). However, Case 13 requires $F(\eta_3) < \eta_3$ $\left(r\gamma_2 < r2\overline{b}_1 + \underline{\gamma}_1 - 2b_2\right)$ while the instability of x_2^* requires $r\gamma_2 > 2b_2$. These two conditions imply $2b_2 < r2\overline{b}_1 + \underline{\gamma}_1 - 2b_2$ that, combined with the further condition $\eta_2 < 0$ $\left(2b_2 > \left(2\underline{b}_1 r + \overline{\gamma}_1\right)\right)$ required by Case 13, leads to $\overline{\gamma}_1 - \underline{\gamma}_1 > 2b_2$. This last condition imply $\overline{\gamma}_1 > 2b_2$ which contradicts $\overline{\gamma}_1 < 2b_2$ (that is $\eta_1 < 0$) required to have Case 13. Therefore, x_2^* is locally-asymptotically stable under Case 13. The global stability follows by noting that

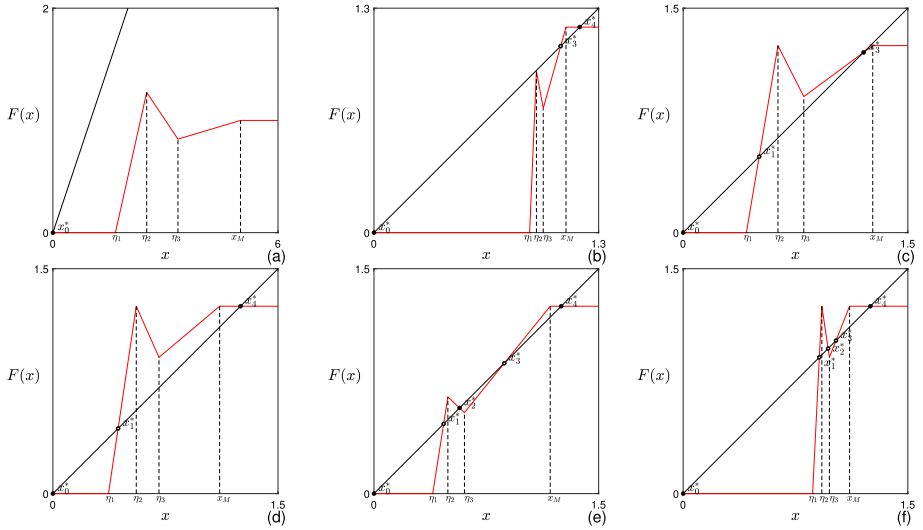

Fig. 1 In red the graph of map F, stable fixed point as a black dot, unstable fixed point as empty black dot. **a** Case 1 in Proposition 3, $b_2 = 0.3$, $\gamma_2 = 0.2$, $\overline{b}_1 = 0.5$, $\underline{b}_1 = 0.1$, $\overline{\gamma}_1 = 0.9$, $\underline{\gamma}_1 = 0.3$. **b** Case 2 in Proposition 3, $b_2 = 0.09$, $\gamma_2 = 0.9$, $\overline{b}_1 = 0.42$, $\underline{b}_1 = 0.1$, $\overline{\gamma}_1 = 0.95$, $\underline{\gamma}_1 = 0.6$. **c**, Case 3 in Proposition 3, $b_2 = 0.3$, $\gamma_2 = 0.79$, $\overline{b}_1 = 0.4$, $\underline{b}_1 = 0.1$, $\overline{\gamma}_1 = 0.9$, $\underline{\gamma}_1 = 0.45$. **d** Case 4 in Proposition 3, $b_2 = 0.3$, $\gamma_2 = 0.9$, $\overline{b}_1 = 0.4$, $\underline{b}_1 = 0.1$, $\overline{\gamma}_1 = 0.9$, $\underline{\gamma}_1 = 0.45$. **e** Case 5(i) in Proposition 3, $b_2 = 0.3$, $\gamma_2 = 0.85$, $\overline{b}_1 = 0.4$, $\underline{b}_1 = 0.1$, $\overline{\gamma}_1 = 0.9$, $\underline{\gamma}_1 = 0.7$. **f** Case 5(ii) in Proposition 3, $b_2 = 0.1$, $\gamma_2 = 0.9$, $\overline{b}_1 = 0.4$, $\underline{b}_1 = 0.1$, $\overline{\gamma}_1 = 0.9$, $\underline{\gamma}_1 = 0.45$. (Color figure online)

$[F(\eta_3), \eta_3]$ is a global absorbing interval an the skew-tent map can used as a normal form for the dynamics of F on this interval.

Consider $\eta_3 < 0$. It follows that the piecewise linear (and continuous) map F is increasing in $[\eta_3, x_M]$ and constant for $x > x_M$. Then, there are 2 possible configurations: Case 14 ($F(x_M) < x_M$) and Case 15 ($F(x_M) > x_M$). The properties (continuity) of F in Proposition 1 and the condition that defines Case 14 imply that x_3^* is the unique equilibrium of F, is attracting in $[0, x_M]$ and each point in (x_M, ∞) is mapped in $\mu_L \in [0, x_M]$ in a single iteration (since $\mu_L = F(x_M) < x_M$). Therefore, x_3^* is globally attracting. The properties (continuity) of F in Proposition 1 and the condition that defines Case 15 imply that x_4^* is the unique equilibrium of F, each point in $[x_M, \infty)$ is mapped in x_4^* in a single iteration and $F(x) > x$ for all $x < x_M$. Therefore, each point outside $[x_M, \infty)$ is mapped inside in a few iterations and x_4^* is globally attracting. This completes the proof. □

The fixed points and the graph of function F in each of the 18 cases identified in Proposition 3 are reported in Figs. 1, 2 and 3. It is worth noting that the results in Proposition 3 reveal that multiple equilibria can exist only when $\eta_1 > 0$, that is, when $\overline{\gamma}_1 > 2b_2$. Note that in the symmetric case analyzed in Radi and Gardini (2023), the function F would not have any multiple and isolated equilibria. Therefore, this is a novelty due to the asymmetric setting.

This is a first relevant observation as the investigation of the fixed points of the one-dimensional map F provides information about the fixed points of the Cournot process given by the decoupled square two-dimensional dynamical map T. Indeed, we have the following results, see Bischi et al. (2000).

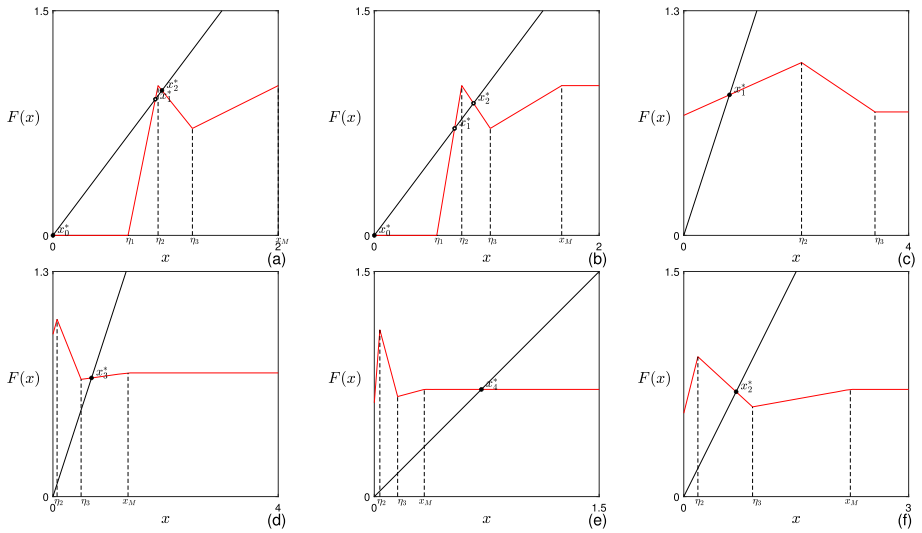

Fig. 2 In red the graph of map F, stable fixed point as a black dot, unstable fixed point as empty black dot. **a** Case 6(i) in Proposition 3, $b_2 = 0.3$, $\gamma_2 = 0.5$, $\overline{b}_1 = 0.5$, $\underline{b}_1 = 0.1$, $\overline{\gamma}_1 = 0.9$, $\underline{\gamma}_1 = 0.45$. **b** Case 6(ii) in Proposition 3, $b_2 = 0.3$, $\gamma_2 = 0.6$, $\overline{b}_1 = 0.5$, $\underline{b}_1 = 0.1$, $\overline{\gamma}_1 = 0.9$, $\underline{\gamma}_1 = 0.45$. **c** Case 7 in Proposition 3, $b_2 = 0.6$, $\gamma_2 = 0.15$, $\overline{b}_1 = 0.7$, $\underline{b}_1 = 0.3$, $\overline{\gamma}_1 = 0.7$, $\underline{\gamma}_1 = 0$. **d** Case 8 in Proposition 3, $b_2 = 0.6$, $\gamma_2 = 0.75$, $\overline{b}_1 = 0.7$, $\underline{b}_1 = 0.2$, $\overline{\gamma}_1 = 0.75$, $\underline{\gamma}_1 = 0.1$. **e** Case 9 in Proposition 3, $b_2 = 0.4$, $\gamma_2 = 3$, $\overline{b}_1 = 0.7$, $\underline{b}_1 = 0.1$, $\overline{\gamma}_1 = 0.7$, $\underline{\gamma}_1 = 0.1$. **f** Case 10(i) in Proposition 3, $b_2 = 0.45$, $\gamma_2 = 0.45$, $\overline{b}_1 = 0.7$, $\underline{b}_1 = 0.1$, $\overline{\gamma}_1 = 0.8$, $\underline{\gamma}_1 = 0.25$. (Color figure online)

Proposition 4 *Consider the one-dimensional map F defined in (21) and the decoupled square two-dimensional map T defined in (16). We have that:*

(i) *x^* is a fixed point of F if and only if $(x^*, R_2(x^*))$ is fixed point of T. The fixed point x^* is locally-asymptotically stable (unstable) for map F if and only if $(x^*, R_2(x^*))$ is locally-asymptotically stable (unstable) for map T.*

(ii) *x^* and x^+ are two fixed points of F if and only if $\left\{\left(x^*, R_2\left(x^+\right)\right); \left(x^+, R_2(x^*)\right)\right\}$ is a 2-cycle of T. The fixed points x^* and x^+ are locally-asymptotically stable (unstable) for map F if and only if $\left\{\left(x^*, R_2\left(x^+\right)\right); \left(x^+, R_2(x^*)\right)\right\}$ is locally-asymptotically stable (unstable) 2-cycle for map T. Moreover, x^* and x^+ are one stable and one unstable if and only if $\left\{\left(x^*, R_2\left(x^+\right)\right); \left(x^+, R_2(x^*)\right)\right\}$ is a saddle 2-cycle for map T.*

(iii) *$\left\{x^+, x^*\right\}$ is a 2-period cycle of F if and only if $\left\{\left(x^+, R_2\left(x^+\right)\right); \left(x^*, R_2\left(x^+\right)\right); \left(x^*, R_2(x^*)\right); \left(x^+, R_2(x^*)\right)\right\}$ is a 4-cycle of T. The 2-period cycle $\left\{x^+, x^*\right\}$ is locally-asymptotically stable (unstable) for map F if and only if $\left\{\left(x^+, R_2\left(x^+\right)\right); \left(x^*, R_2\left(x^+\right)\right); \left(x^*, R_2(x^*)\right); \left(x^+, R_2(x^*)\right)\right\}$ is locally-asymptotically stable (unstable) 4-cycle for map T.*

(iv) *$\{x_1, x_2, x_3\}$ is an 3-cycle of F if and only if*

$$C_1 = \{(x_1, y_1), (x_2, y_1), (x_2, y_2), (x_3, y_2), (x_3, y_3), (x_1, y_3)\}$$
$$\text{and} \quad C_2 = \{(x_1, y_2), (x_3, y_1), (x_2, y_3)\} \tag{33}$$

are, respectively, a 6-cycle and a 3-cycle of T, where $\{y_1, \ldots, y_n\} = \{R_2(x_1), \ldots, R_2(x_n)\}$. The 3-period cycle $\{x_1, x_2, x_3\}$ is locally-asymptotically stable (unstable) for map F if

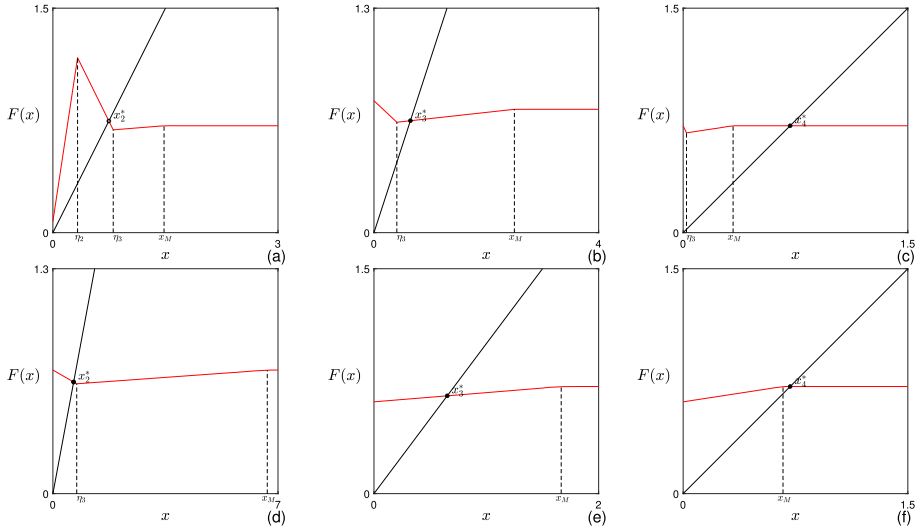

Fig. 3 In red the graph of map F, stable fixed point as a black dot, unstable fixed point as empty black dot. **a** Case 10(ii) in Proposition 3, $b_2 = 0.33$, $\gamma_2 = 0.675$, $\overline{b}_1 = 0.7$, $\underline{b}_1 = 0.1$, $\overline{\gamma}_1 = 0.65$, $\underline{\gamma}_1 = 0.055$. **b** Case 11 in Proposition 3, $b_2 = 0.6$, $\gamma_2 = 0.4$, $\overline{b}_1 = 0.7$, $\underline{b}_1 = 0.1$, $\overline{\gamma}_1 = 0.7$, $\underline{\gamma}_1 = 0.15$. **c** Case 12 in Proposition 3, $b_2 = 0.7$, $\gamma_2 = 3$, $\overline{b}_1 = 0.7$, $\underline{b}_1 = 0.1$, $\overline{\gamma}_1 = 0.7$, $\underline{\gamma}_1 = 0.1$. **d** Case 13 in Proposition 3, $b_2 = 0.6$, $\gamma_2 = 0.15$, $\overline{b}_1 = 0.7$, $\underline{b}_1 = 0.0$, $\overline{\gamma}_1 = 0.75$, $\underline{\gamma}_1 = 0.15$. **e** Case 14 in Proposition 3, $b_2 = 0.7$, $\gamma_2 = 0.6$, $\overline{b}_1 = 0.7$, $\underline{b}_1 = 0.0$, $\overline{\gamma}_1 = 0.6$, $\underline{\gamma}_1 = 0.2$. **f** Case 15 in Proposition 3, $b_2 = 0.7$, $\gamma_2 = 1.5$, $\overline{b}_1 = 0.7$, $\underline{b}_1 = 0.0$, $\overline{\gamma}_1 = 0.6$, $\underline{\gamma}_1 = 0.2$. (Color figure online)

and only if C_1 and C_2 are locally-asymptotically stable (unstable) 6-cycle and 3-cycle for map T.

(v) *$\{x_1, \ldots, x_n\}$ is an n-cycle of F if and only if $\{x_1, \ldots, x_n\} \times \{y_1, \ldots, y_n\}$ is a set of periodic points of T that includes (among others) the $2n$-cycle of T given by $\{(x_1, y_1), (x_2, y_1), (x_2, y_2), \ldots, (x_{n-1}, y_{n-1}), (x_n, y_n)\}$, where $\{y_1, \ldots, y_n\} = \{R_2(x_1), \ldots, R_2(x_n)\}$. The n-period cycle $\{x_1, \ldots, x_n\}$ is locally-asymptotically stable (unstable) for map F if and only if $\{(x_1, y_1), (x_2, y_1), (x_2, y_2), \ldots, (x_{n-1}, y_{n-1}), (x_n, y_n)\}$ is locally-asymptotically stable (unstable) $2n$-cycle for map T.*

The results in Proposition 4 can be used to describe the quantity dynamics of the duopoly game with ambiguity aversion in each of the 18 cases identified in Proposition 3.

Specifically, for the Case 1 of Proposition 3, the graph of map F is depicted in Fig. 1a while the (associated) dynamics of the map T is depicted in Fig. 4a. Looking at the parameter conditions that identify Case 1, we have $\overline{\gamma}_1 > 2b_2$, that is firm 1 considers possible that the production of the competitor has a significant impact on the market price of its goods, and $\gamma_2 < 2\overline{b}_1$, that is firm 2 considers possible only a lower impact of the production of the competitor on the market price of its goods.[11] Looking at the dynamics of the duopoly, we

[11] Considering the symmetric setting $a = a_1 - c_1 = a_2 - c_2 = 1$ and m any positive integer number greater than 1, we interpret and/or justify $\overline{\gamma}_1 > mb_2$ as firm 1's worst-case belief that new competitors enter the oligopoly at the current time and the number of competitors are m instead of 1 as it is in a duopoly game. The more stringent condition $\underline{\gamma}_1 > mb_2$ is motivated as firm 1's belief that the number of competitors (in all the worst-case configurations) can be more than m in the next period. At the same time, we interpret and/or justify $\gamma_2 > m\overline{b}_1$ and $\gamma_2 > m\underline{b}_1$ as firm 2's belief that the number of competitors (in the worst-case configuration) can be more than m in the next period.

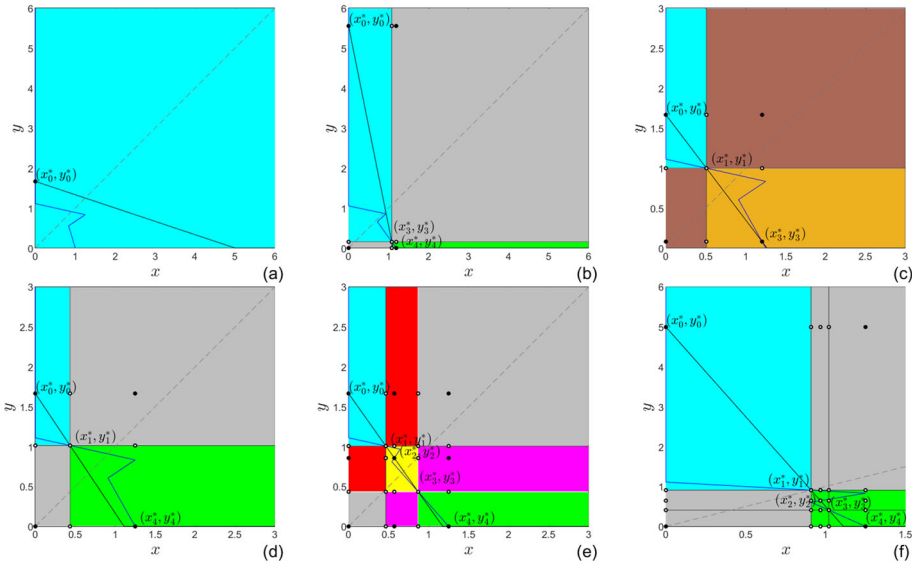

Fig. 4 In cyan the basin of attraction of $\left(x_0^*, y_0^*\right)$. In yellow the basin of attraction of $\left(x_2^*, y_2^*\right)$. In orange the basin of attraction of $\left(x_3^*, y_3^*\right)$. In green the basin of attraction of $\left(x_4^*, y_4^*\right)$. In gray the basin of attraction of the 2-cycle $\left\{\left(x_0^*, y_4^*\right); \left(x_4^*, y_0^*\right)\right\}$. In red the basin of attraction of the 2-cycle $\left\{\left(x_0^*, y_2^*\right); \left(x_2^*, y_0^*\right)\right\}$. In brown the basin of attraction of the 2-cycle $\left\{\left(x_0^*, y_3^*\right); \left(x_3^*, y_0^*\right)\right\}$. In magenta the basin of attraction of the 2-cycle $\left\{\left(x_2^*, y_4^*\right); \left(x_4^*, y_2^*\right)\right\}$. In blue the graph of $R_1(y)$, in black the graph of $R_2(x)$. **a** Case 1 in Proposition 3, $b_2 = 0.3, \gamma_2 = 0.2, \overline{b}_1 = 0.5, \underline{b}_1 = 0.1, \overline{\gamma}_1 = 0.9, \underline{\gamma}_1 = 0.3$. **b** Case 2 in Proposition 3, $b_2 = 0.09, \gamma_2 = 0.9, \overline{b}_1 = 0.42, \underline{b}_1 = 0.1, \overline{\gamma}_1 = 0.95, \underline{\gamma}_1 = 0.6$. **c** Case 3 in Proposition 3, $b_2 = 0.3, \gamma_2 = 0.79, \overline{b}_1 = 0.4, \underline{b}_1 = 0.1, \overline{\gamma}_1 = 0.9, \underline{\gamma}_1 = 0.45$. **d** Case 4 in Proposition 3, $b_2 = 0.3, \gamma_2 = 0.9, \overline{b}_1 = 0.4, \underline{b}_1 = 0.1, \overline{\gamma}_1 = 0.9, \underline{\gamma}_1 = 0.45$. **e** Case 5(i) in Proposition 3, $b_2 = 0.3, \gamma_2 = 0.85, \overline{b}_1 = 0.4, \underline{b}_1 = 0.1, \overline{\gamma}_1 = 0.9, \underline{\gamma}_1 = 0.7$. **f** Case 5(ii) in Proposition 3, $b_2 = 0.1, \gamma_2 = 0.9, \overline{b}_1 = 0.4, \underline{b}_1 = 0.1, \overline{\gamma}_1 = 0.9, \underline{\gamma}_1 = 0.45$. (Color figure online)

observe that the equilibrium $\left(x_0^*, y_0^*\right)$ is globally stable (its basin of attraction is depicted in cyan in Fig. 4a). Noting that $x_0^* = 0$ and $y_0^* > 0$, we have that in the long run firm 2 produces while firm 1 is out of the market. Specifically, firm 1 faces uncertainty that inhibits production.

The graph of map F in Fig. 1b and the dynamics of map T in Fig. 4b refer to the Case 2 of Proposition 3. Looking at the parameter conditions that identify Case 2, we have $\overline{\gamma}_1 > 2b_2$ and $\gamma_2 > 2\overline{b}_1$, that is both firms 1 and 2 consider the possibility that the market price of their own goods is highly sensitive to the production of the competitors. In this case, Fig. 4b confirms that the stable equilibria are $\left(x_0^*, y_0^*\right)$ and $\left(x_4^*, y_4^*\right)$. Depending on the initial conditions, we have that either firm 2 (if we converge to $\left(x_0^*, y_0^*\right)$) or firm 1 (if we converge to $\left(x_4^*, y_4^*\right)$) survives in the market. However, there is also a stable 2-cycle $\left\{\left(x_0^*, y_4^*\right), \left(x_4^*, y_0^*\right)\right\}$ and its basin of attraction is depicted in gray in Fig. 4b. Converging to this 2-cycle, we have that both firms produce once every two periods.

A similar dynamics is observed for Case 3 of Proposition 3. The graph of map F is depicted in Fig. 1c and the dynamics of the map T in Fig. 4c. We observe that there are two stable equilibria $\left(x_0^*, y_0^*\right)$ (basin of attraction in cyan) and $\left(x_3^*, y_3^*\right)$ (basin of attraction in brown) and a stable 2-cycle $\left\{\left(x_0^*, y_3^*\right), \left(x_3^*, y_0^*\right)\right\}$ (basin of attraction in magenta). The

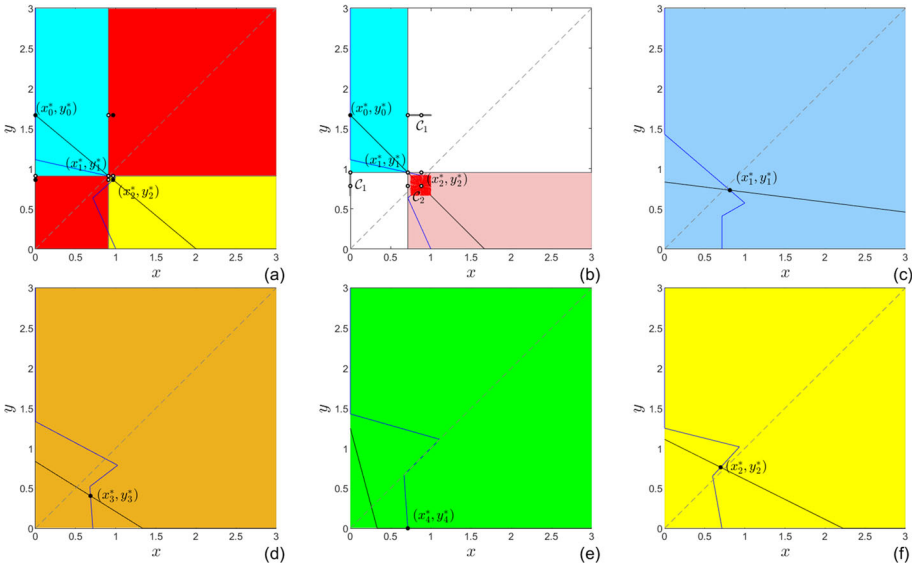

Fig. 5 In dark gray the 2-pieces chaotic attractor $\mathcal{C}_1$. In red the one-piece chaotic attractor $\mathcal{C}_2$. In cyan the basin of attraction of $\left(x_0^*, y_0^*\right)$. In sky-blue the basin of attraction of $\left(x_1^*, y_1^*\right)$. In yellow the basin of attraction of $\left(x_2^*, y_2^*\right)$. In orange the basin of attraction of $\left(x_3^*, y_3^*\right)$. In green the basin of attraction of $\left(x_4^*, y_4^*\right)$. In red the basin of attraction of the 2-cycle $\left\{\left(x_0^*, y_2^*\right); \left(x_2^*, y_0^*\right)\right\}$. In white the basin of attraction of $\mathcal{C}_1$. In pink the basin of attraction of $\mathcal{C}_2$. In blue the graph of $R_1(y)$, in black the graph of $R_2(x)$. **a** Case 6(i) in Proposition 3, $b_2 = 0.3$, $\gamma_2 = 0.5$, $\overline{b}_1 = 0.5$, $\underline{b}_1 = 0.1$, $\overline{\gamma}_1 = 0.9$, $\underline{\gamma}_1 = 0.45$. **b** Case 6(ii) in Proposition 3, $b_2 = 0.3$, $\gamma_2 = 0.6$, $\overline{b}_1 = 0.5$, $\underline{b}_1 = 0.1$, $\overline{\gamma}_1 = 0.9$, $\underline{\gamma}_1 = 0.45$. **c** Case 7 in Proposition 3, $b_2 = 0.6$, $\gamma_2 = 0.15$, $\overline{b}_1 = 0.7$, $\underline{b}_1 = 0.3$, $\overline{\gamma}_1 = 0.7$, $\underline{\gamma}_1 = 0$. **d** Case 8 in Proposition 3, $b_2 = 0.6$, $\gamma_2 = 0.75$, $\overline{b}_1 = 0.7$, $\underline{b}_1 = 0.2$, $\overline{\gamma}_1 = 0.75$, $\underline{\gamma}_1 = 0.1$. **e** Case 9 in Proposition 3, $b_2 = 0.4$, $\gamma_2 = 3$, $\overline{b}_1 = 0.7$, $\underline{b}_1 = 0.1$, $\overline{\gamma}_1 = 0.7$, $\underline{\gamma}_1 = 0.1$. **f** Case 10(i) in Proposition 3, $b_2 = 0.45$, $\gamma_2 = 0.45$, $\overline{b}_1 = 0.7$, $\underline{b}_1 = 0.1$, $\overline{\gamma}_1 = 0.8$, $\underline{\gamma}_1 = 0.25$. (Color figure online)

dynamics is therefore very similar to the one of Case 2. However, in any of the three possible attractors of Case 3 the level of production of firm 2 is always positive. This is justified by the parameter restrictions that identify Case 3. Indeed, as in Case 1 we have $\overline{\gamma}_1 > 2b_2$ and $\gamma_2 < 2\overline{b}_1$, that is firm 1 believes that the market price of its goods is highly sensitive to the level of production of competitor while firm 2 believes that the market price of its production is less sensitive to the output of the competitor. As opposed to Case 1, in Case 3 we have $\left(\overline{\gamma}_1 - 2b_2\right) < r\left(\gamma_2 - 2\underline{b}_1\right)$, which implies $\gamma_2 > 2\underline{b}_1$. This *pessimistic* belief of firm 2 favors its competitor in the sense that $\left(x_0^*, y_0^*\right)$ (where firm 2 dominates the market, it is a monopolist) is not a globally attractor, as it is in Case 1, and an attracting equilibrium where firm 1 produces more than firm 2 exists and is given by $\left(x_3^*, y_3^*\right)$.

Analogous to that of Case 2, is the dynamics in Case 4. See Fig. 4d. The only difference is the equilibrium $\left(x_1^*, y_1^*\right)$ that substitutes $\left(x_3^*, y_3^*\right)$ in separating (through its manifolds) the basins of attraction of the locally-asymptotically stable equilibria $\left(x_0^*, y_0^*\right)$ and $\left(x_4^*, y_4^*\right)$ and the stable 2-cycle $\left\{\left(x_0^*, y_4^*\right), \left(x_4^*, y_0^*\right)\right\}$. Instead, the Case 5(i) is more complicated. Specifically, we have a stable inner equilibrium $\left(x_2^*, y_2^*\right)$ where both firms have a positive level of production. Its basin of attraction is depicted in yellow in Fig. 4e. In addition to that, we have the stable equilibria $\left(x_0^*, y_0^*\right)$ and $\left(x_4^*, y_4^*\right)$ where firm 1, resp. firm 2, does not produce. Finally, we have three 2-cycles that coexist and are stable, that is $\left\{\left(x_0^*, y_4^*\right), \left(x_4^*, y_0^*\right)\right\}$ (basin of attrac-

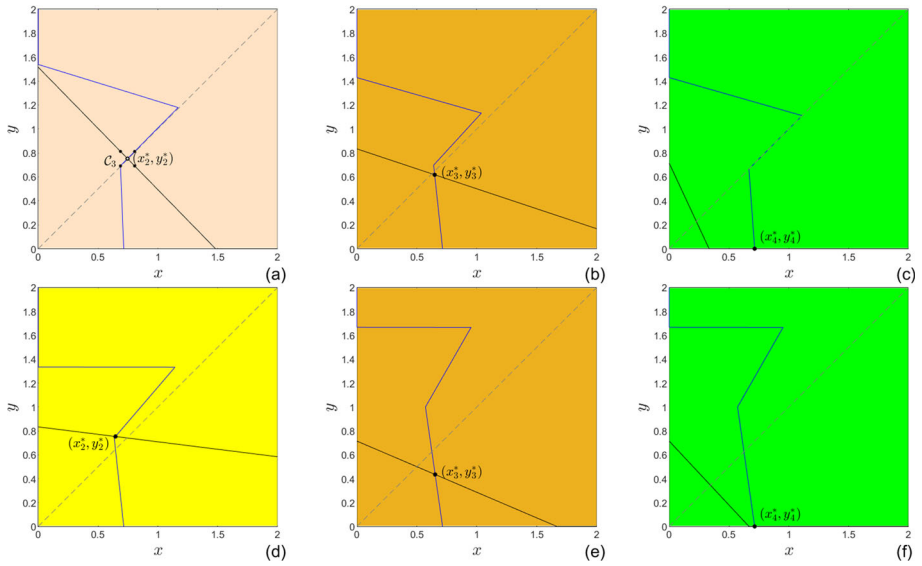

Fig. 6 In black the attracting 4-cycle $\mathcal{C}_3$. In bisque the basin of attraction of the 4-cycle $\mathcal{C}_3$. In yellow the basin of attraction of $\left(x_2^*, y_2^*\right)$. In orange the basin of attraction of $\left(x_3^*, y_3^*\right)$. In green the basin of attraction of $\left(x_4^*, y_4^*\right)$. In blue the graph of R_1 (y), in black the graph of R_2 (x). **a** Case 10(ii) in Proposition 3, $b_2 = 0.33$, $\gamma_2 = 0.675$, $\overline{b}_1 = 0.7$, $\underline{b}_1 = 0.1$, $\overline{\gamma}_1 = 0.65$, $\underline{\gamma}_1 = 0.055$. **b** Case 11 in Proposition 3, $b_2 = 0.6$, $\gamma_2 = 0.4$, $\overline{b}_1 = 0.7$, $\underline{b}_1 = 0.1$, $\overline{\gamma}_1 = 0.7$, $\underline{\gamma}_1 = 0.15$. **c** Case 12 in Proposition 3, $b_2 = 0.7$, $\gamma_2 = 3$, $\overline{b}_1 = 0.7$, $\underline{b}_1 = 0.1$, $\overline{\gamma}_1 = 0.7$, $\underline{\gamma}_1 = 0.1$. **d** Case 13 in Proposition 3, $b_2 = 0.6$, $\gamma_2 = 0.15$, $\overline{b}_1 = 0.7$, $\underline{b}_1 = 0.0$, $\overline{\gamma}_1 = 0.75$, $\underline{\gamma}_1 = 0.15$. **e** Case 14 in Proposition 3, $b_2 = 0.7$, $\gamma_2 = 0.6$, $\overline{b}_1 = 0.7$, $\underline{b}_1 = 0.0$, $\overline{\gamma}_1 = 0.6$, $\underline{\gamma}_1 = 0.2$. **f** Case 15 in Proposition 3, $b_2 = 0.7$, $\gamma_2 = 1.5$, $\overline{b}_1 = 0.7$, $\underline{b}_1 = 0.0$, $\overline{\gamma}_1 = 0.6$, $\underline{\gamma}_1 = 0.2$. (Color figure online)

tion in gray), $\left\{\left(x_2^*, y_4^*\right), \left(x_4^*, y_2^*\right)\right\}$ (basin of attraction in magenta) and $\left\{\left(x_0^*, y_2^*\right), \left(x_2^*, y_0^*\right)\right\}$ (basin of attraction in red). Moving from Case 5(i) to Case 5(ii), the inner equilibrium $\left(x_2^*, y_2^*\right)$, as well as the 2-cycles $\left\{\left(x_2^*, y_4^*\right), \left(x_4^*, y_2^*\right)\right\}$ and $\left\{\left(x_0^*, y_2^*\right), \left(x_2^*, y_0^*\right)\right\}$, lose stability. As stated in Proposition 3, in Case 5(ii) the dynamics of F can be of different types: (1) characterized by a locally-asymptotically stable cycle; (2) characterized by a chaotic attractor; (3) characterized by a chaotic repellor. This last case is the one related to the constellation of parameter values of Fig. 1f. This configuration mirrors in a dynamics for map T where there are three attractors, that is the equilibria $\left(x_4^*, y_4^*\right)$ and $\left(x_0^*, y_0^*\right)$ and the 2-cycle $\left\{\left(x_0^*, y_4^*\right), \left(x_4^*, y_0^*\right)\right\}$. Specifically, the basin of attraction of $\left(x_4^*, y_4^*\right)$ includes a region that would be the basin of attraction of $\left(x_2^*, y_2^*\right)$ if it were stable and a region that would be the basin of attraction of $\left\{\left(x_2^*, y_4^*\right), \left(x_4^*, y_2^*\right)\right\}$ if it were stable. At the same time, the basin of attraction of the 2-cycle $\left\{\left(x_0^*, y_4^*\right), \left(x_4^*, y_0^*\right)\right\}$ includes also a region that would be the basin of $\left\{\left(x_0^*, y_2^*\right), \left(x_2^*, y_0^*\right)\right\}$ if it were stable. See Fig. 1f. Therefore, the dynamics of Case 5(ii) is analogous to the one of Cases 4 and 2 despite $\underline{\gamma}_1 > 2b_2$ (firm 1 has a very conservative belief in Case 5(ii), that is, it considers a very high sensitivity of the market price of its goods to the level of production of the competitor). The other possible dynamic configurations related to Case 5(ii) are analyzed in the following.

For the values of parameters as in Case 6(i) of Proposition 3, we have the stable equilibrium $\left(x_0^*, y_0^*\right)$ that coexists with the stable equilibrium $\left(x_2^*, y_2^*\right)$, where both firms have a positive level of production, and with the stable 2-cycle $\left\{\left(x_0^*, y_2^*\right), \left(x_2^*, y_0^*\right)\right\}$. See Fig. 5a. Note that

under Case 6(i) firm 2 considers the possibility that the market price of its goods is not highly sensitive to the level of production of the competitor, that is $\gamma_2 < 2\overline{b}_2$, and the level of production of firm 2 is always positive in the long run. Moving to Case 6(ii), the inner equilibrium $\left(x_2^*, y_2^*\right)$ loses stability and a stable chaotic attractor $\mathcal{C}_2$ appears. At the same time, the 2-cycle $\left\{\left(x_0^*, y_2^*\right), \left(x_2^*, y_0^*\right)\right\}$ loses stability and a 2-pieces chaotic attractor $\mathcal{C}_1$ appears. See Fig. 5b. Let us remark that moving from Case 6(i) to Case 6(ii), the loss of stability of the equilibrium $\left(x_2^*, y_2^*\right)$ occurs through a degenerate-flip bifurcation and either a stable cycle or a chaotic repellor may appear instead of a chaotic attractor. These other possible dynamic configurations related to Case 6(ii) are analyzed in the following.

In all the remaining cases, we have $\overline{\gamma}_1 < 2b_2$. That is, firm 1 considers as a worst case a lower sensitivity of the market price of its products to the production of the competitor. As a result we have that in all the remaining cases $\left(x_0^*, y_0^*\right)$ is not anymore an equilibrium and the level of production of firm 1 is always positive in the long run.

Specifically, in Cases 7 and 8 of Proposition 3, we have that both firms believe that the market price of their goods cannot be highly sensitive with respect to the level of production of the competitors ($\overline{\gamma}_1 < 2b_2$ and $\gamma_2 < 2\overline{b}_1$) and we have a unique and globally stable inner equilibrium given by $\left(x_1^*, y_1^*\right)$ and $\left(x_3^*, y_3^*\right)$, respectively. Their basins of attraction are depicted in sky-blue and in orange in Fig. 5c, d, respectively.

In Case 9 of Proposition 3, we have that firm 2 believes that the market price of its goods is very sensitive to the level of production of the competitor, that is $\gamma_2 > 2\overline{b}_2$, and this brings to the globally stable equilibrium $\left(x_4^*, y_4^*\right)$, see the green region in Fig. 5e, where firm 2 is forced not to produce due to strong uncertainty. The dynamics of map T in Case 10(i) of Proposition 3 is similar to the ones in Cases 7 and 8, in the sense that there is a unique inner equilibrium, in this case $\left(x_2^*, y_2^*\right)$, which is globally stable and where both firms have a positive level of production. Its basin of attraction is depicted in yellow in Fig. 5f. We note that both firms believe that the market price of their goods is not highly sensitive to the level of production of the competitor in all Cases 7, 8 and 10(i). However, increasing the value of γ_2 we have the loss of stability of $\left(x_2^*, y_2^*\right)$. It is the Case 10(ii) of Proposition 3. Then, a periodic cycle around $\left(x_2^*, y_2^*\right)$ may appear and it is globally stable. As it is the 4-cycle depicted in Fig. 6a. Case 10(ii) is a very peculiar case as it identifies the only parameter configurations (configurations of the uncertainty sets) for which a cycles is the unique attractor. Let us remark that moving from Case 10(i) to Case 10(ii), either a chaotic attractor or a chaotic repellor may appear instead of a stable cycle. These other possible dynamic configurations related to Case 10(ii) are analyzed in the following.

In all the other cases where firm 2 believes that the market price of its goods is not highly sensitive to the level of production of the competitor, belief represented by the condition $\gamma_2 > 2\overline{b}_1$, we have that $\left(x_4^*, y_4^*\right)$ is the unique globally attracting equilibrium and firm 2 does not produce in the long run. They are Cases 12 and 15 in Fig. 6c, f. Instead in all the remaining cases, we have that firm 2 also believes that the number of competitors are less than two, as identified by the condition $\gamma_2 < 2\overline{b}_1$, and we have a unique globally stable inner equilibrium, that is, either $\left(x_2^*, y_2^*\right)$ or $\left(x_3^*, y_3^*\right)$. They are Cases 11, 13 and 14. See Fig. 6b, d, e.

Summarizing, we observe that $\left(x_0^*, y_0^*\right)$, where firm 1 does not produce, exists and is stable when firm 1 believes that the market price of its product is highly sensitive to the level of production of the competitor, that is $\overline{\gamma}_1 > 2b_2$. At the same time, $\left(x_4^*, y_4^*\right)$, where firm 2 does not produce, exists and is stable when firm 2 believes that the market price of its product is highly sensitive to the level of production of the competitor, that is $\gamma_2 > 2\overline{b}_1$. Moreover, we observe that when both firms believe in a market price that is highly sensitivity to the level of production of the competitor, we have that $\left(x_0^*, y_0^*\right)$ and $\left(x_4^*, y_4^*\right)$ coexist and

are stable equilibria. Therefore, there is the possibility that a firm does not produce in the long run. Moreover, these two equilibria coexist with a stable 2-cycle where firms alternate a period in which both do not produce and a period in which they produce. Finally, only inner equilibria $\left(x_1^*, y_1^*\right)$, $\left(x_2^*, y_2^*\right)$ and $\left(x_3^*, y_3^*\right)$ exist when both firms consider possible only a limited sensitivity of the market price of their goods with respect to the level of production of the competitor, that is: $\overline{\gamma}_1 < 2b_2$ and $\gamma_2 < 2\overline{b}_1$.

Another common factor is the emergence of either chaotic attractors or stable cycles of periodicity higher than 2. This occurs always when $\left(x_2^*, y_2^*\right)$ losses stability, i.e. it requires the condition $r\gamma_2 > 2b_2$.

4 Bifurcation analysis

This section is devoted to analyze the border-collision bifurcations through which we move from one case to another of those described in Proposition 3 and the bifurcations through which periodic and chaotic attractors appear and disappear. We use γ_2 and $\overline{\gamma}_1$ as the bifurcation parameters as they define the degree of competition in the duopoly. Moreover, we focus on three different scenarios (constellations of the values of the non-bifurcation parameters) that allows us to discuss the main bifurcations and global dynamics that can be generated by the duopoly game. Different constellation parameters and bifurcation curves are analyzed in Radi and Gardini (2023), which confirm the current results and underline the super stable periodic solutions, which occurs when a periodic point is in the flat branch of the map.[12]

4.1 Scenario 1

Let us start considering the following values of the non-bifurcation parameters

$$\overline{b}_1 = 2, \quad \underline{b}_1 = 0.3, \quad \underline{\gamma}_1 = 0.2, \quad b_2 = 0.7 \tag{34}$$

and let us analyze for the cases identified in Proposition 3 their distribution in the parameter plane $\left(\overline{\gamma}_1, \gamma_2\right)$ in Fig. 7a, where $\overline{\gamma}_1$ varies in $\left(\underline{\gamma}_1, 5\right) = (0.2, 5)$ and γ_2 varies in $(0, 5)$.

For the parameter constellation as in (34) and $\eta_3 < 0$ we have either Case 14 or Case 15, see Proposition 3. As shown in Fig. 7a, increasing $\overline{\gamma}_1$ to have η_3 positive, we move from Case 14 to Case 11, and the unique equilibrium x_3^* of F persists globally stable, and from Case 15 to Case 12, and the unique equilibrium x_4^* of F persists globally stable. Therefore, neither bifurcations nor persistence border collisions occur by moving from Case 15 to Case 12 and from Case 14 to Case 11. At the same time, for parameters as in (34) and $\eta_2 < 0 < \eta_3$, we can have only Cases 11, 12 and 13, see Proposition 3. Increasing $\overline{\gamma}_1$ in order to have $\eta_2 > 0$, from Case 11 we enter Case 8 and in both regions we have that the unique equilibrium of F is x_3^* and is globally stable. Similarly, from Case 13 we enter Case 10(i) by increasing $\overline{\gamma}_1$ and in both regions we have that the unique equilibrium of F is x_2^* and is globally stable. Finally, from Case 12 we enter Case 9 by increasing $\overline{\gamma}_1$ and even in this case the unique equilibrium of F remains x_4^* and is globally stable. Therefore, neither bifurcations nor border collisions occur crossing the border between Case 13 and Case 10(i), the border between Case 11 and Case 8 and the border between Case 12 and Case 9. For this reason, these borders are not marked anymore in the following.

[12] As a further addition to Radi and Gardini (2023), Sect. 3 provides a classification of all possible configurations of equilibria while Sect. 4 shows the existence of periodic and chaotic dynamics for constellation parameters consistent with a duopoly game without the threat of new entry.

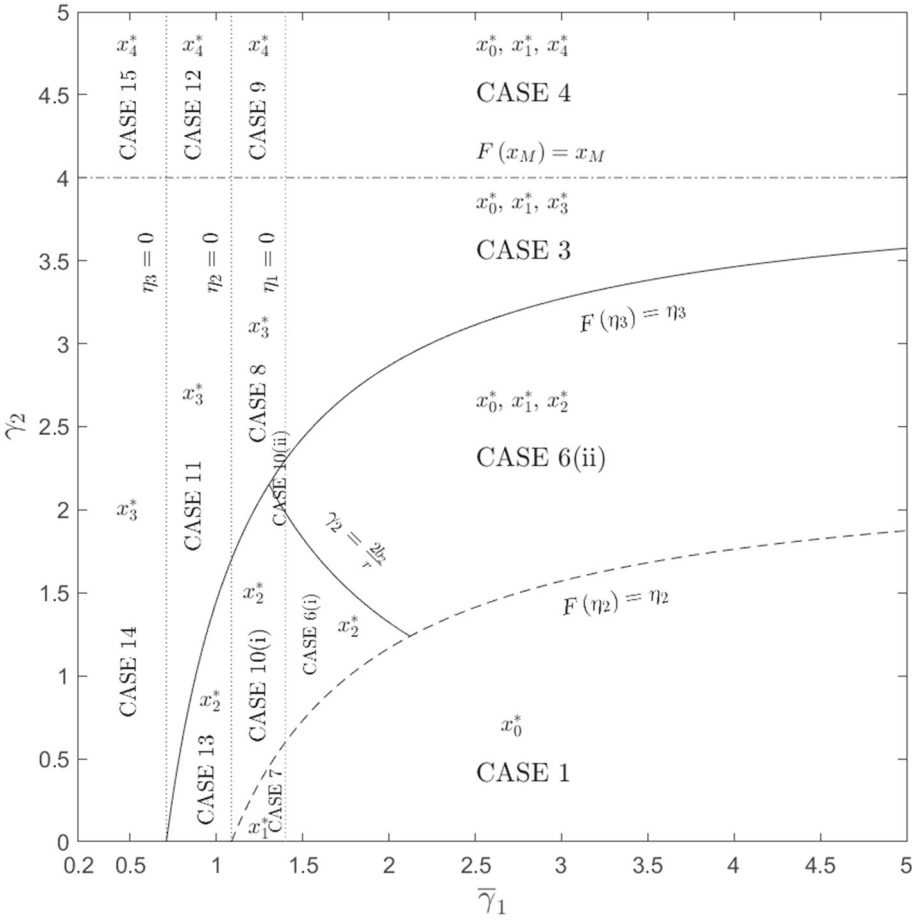

Fig. 7 Parameter plane $\overline{\gamma}_1 - \gamma_2$ showing the borders of the regions representing the cases identified in Proposition 3. Parameters: $(\overline{\gamma}_1, \gamma_2) \in [0.2, 5] \times [0, 5]$ and the remaining ones as in (34). (Color figure online)

Moreover, crossing the curve $F(x_M) = x_M$ ($\gamma_2 < 2\overline{b}_1$) by increasing γ_2 we have one of the following four possibilities: A) move from Case 3 to Case 4; B) move from Case 8 to Case 9; C) move from Case 11 to Case 12; D) move from Case 14 to Case 15. In all these cases, we have that the globally stable equilibrium x_4^* appears instead of the globally stable equilibrium x_3^*. Therefore, the border collisions that occur crossing the line $\gamma_2 = 2\overline{b}_1$ do not produce bifurcations that change the qualitative nature of the global dynamics of the map F. For this region, in the following we focus on the region $\gamma_2 < 2\overline{b}_1$, see Fig. 7b, and we first analyze the bifurcations and the global dynamics of F and afterward the one of T.

4.1.1 Scenario 1: bifurcations and global dynamics of *F*

Let us consider F and let us analyze the two-dimensional bifurcation diagram of Fig. 8a for which the related distribution of the cases identified in Proposition 3 is in Fig. 8b. Looking at the two-dimensional bifurcation diagram of Fig. 8a we observe the brown-yellow region

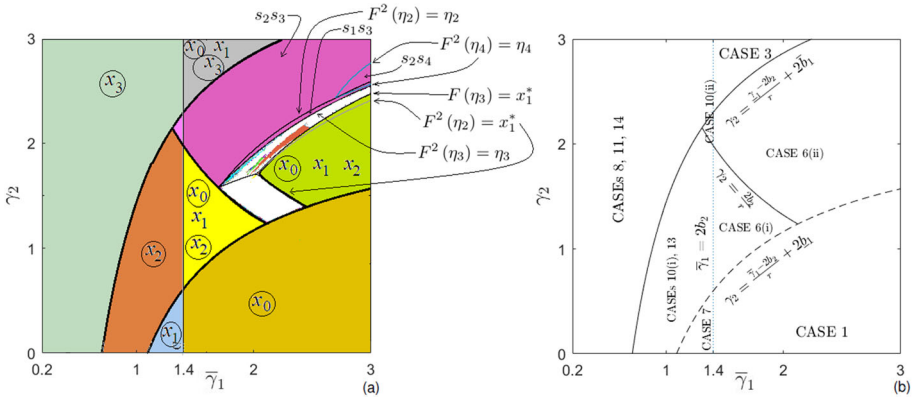

Fig. 8 **a** Two-dimensional bifurcation diagrams showing the dynamics in the parameter plane $\overline{\gamma}_1 - \gamma_2$. Magenta indicates a 2-cycle for F (4-cycle for T), red indicates a 3-cycle for F (6-cycle for T), azure indicates a 4-cycle for F (8-cycle for T), green indicates a 5-cycle for F (10-cycle for T). **b** Parameter plane $\overline{\gamma}_1 - \gamma_2$ showing the borders of the regions representing the cases identified in Proposition 3. Parameters: $(\overline{\gamma}_1, \gamma_2) \in [0.2, 3] \times [0, 3]$ and the remaining ones as in (34). The equilibria x_i^* are indicated as x_i for the sake of simplicity of notation. (Color figure online)

(Case 1) where the unique and globally stable equilibrium is x_0^*, the light-green region (Cases 8, 11 and 14) where the unique and globally stable equilibrium is x_3^*, the light-blue region (Case 7) where the unique and globally stable equilibrium is x_1^* and the orange region (Cases 10(i) and 13) where the unique and globally stable equilibrium is x_2^*.

The light-magenta region [Case 10(ii)] is also a region of the parameter space characterized by a unique equilibrium given by x_2^* which, however, is unstable. Almost all trajectories are attracted by a 2-period cycle that surrounds x_2^*. Then, the light-magenta region is small but very peculiar as it is the only region of the parameter space where only periodic dynamics are attracting, that is, where locally-asymptotically stable equilibria are not present.

The remaining regions of the parameter space are characterized by three equilibria. Specifically, in the gray region (Case 3) the equilibria are x_0^*, x_1^* and x_3^*, and only x_0^* and x_3^* are locally-asymptotically stable. In the yellow region [Case 6(i)] the equilibria are x_0^*, x_1^* and x_2^*, and x_1^* is unstable while the other two are locally-asymptotically stable. In the white region [Case 6(ii)], there are the same equilibria x_0^*, x_1^* and x_2^* but only x_0^* is locally-asymptotically stable and coexists with a chaotic attractor. In the green region [Case 6(ii)] the equilibria remain x_0^*, x_1^* and x_2^*, but x_0^* coexists with a chaotic repellor and it is almost globally stable. Finally, we have the regions depicted in magenta, azure, red and so on [Case 6(ii)]. In these regions the equilibria remain x_0^*, x_1^* and x_2^*, and x_0^* is the only locally-asymptotically stable equilibrium that coexists with a periodic attractor. Figure 9a shows, for example, a configuration of F where a locally-asymptotically stable 3-cycle coexists with the superstable equilibrium x_0^*.

Let us now analyze the persistence border-collision and bifurcation curves. Let us start with the border collision curve $x_0^* = x_1^*$ (also $\eta_1 = 0$ or $\overline{\gamma}_1 < 2b_2$) at which the two equilibria x_0^* and x_1^* merge in the kink point $\eta_1 = 0$. Marking the border between light-green and gray regions and between orange and light-yellow regions, this curve identifies a fold border-collision bifurcation at which x_0^* (superstable) and x_1^* (unstable) appear (increasing $\overline{\gamma}_1$). Underlining the edge between light-blue and brown-yellow regions, the same curve identifies instead a persistent border collision bifurcation, where the globally stable equilibrium x_1^*

merges with globally stable equilibrium x_0^* and disappears (increasing $\overline{\gamma}_1$) while x_0^* appears. Finally, marking the edge between light-magenta and magenta regions, this curve identifies a border-collision bifurcation at which the equilibria x_0^* (superstable) and x_1^* (unstable) appear and persist entering the magenta region. Moreover, a two-period cycle of F persists and it is locally-asymptotically stable both in the light-magenta region [Case 10(ii)] and in the magenta region [inside Case 6(ii)].

The curve given by equation $F^2(\eta_2) = \eta_2$ identifies instead a persistent border collision at which a periodic point of the locally-asymptotically stable 2-cycle that we observe only in the magenta region has a contact with the kink point η_2. Inside this magenta region and above this curve, the 2-cycle has either a symbolic sequence $\sigma_2\sigma_3$ and is stable (if we are outside the region bounded by the two pieces of the curve $F^2(\eta_4) = \eta_4$), or a symbolic sequence $\sigma_2\sigma_4$ and is superstable (if we are inside the region bounded by the two pieces of the curve $F^2(\eta_4) = \eta_4$). Inside the same magenta region but below this curve, the symbolic sequence changes either in $\sigma_1\sigma_3$ and the 2-cycle remains stable (if we are outside the region bounded by the two pieces of the curve $F^2(\eta_4) = \eta_4$), or in $\sigma_1\sigma_4$ and the 2-cycle remains superstable (if we are inside the region bounded by the two pieces of the curve $F^2(\eta_4) = \eta_4$). That is, this curve identifies a persistent border collision at which a periodic point of the 2-cycle has a contact with the kink point η_2.

The two pieces of the already mention border collision curve $F^2(\eta_4) = \eta_4$ marks a bounded subregion of the magenta region. Entering this subregion, a periodic point of the locally-asymptotically stable 2-cycle that we observe in the magenta region has a contact with the kink point η_4. Inside this subregion, one periodic point of this 2-cycle involves the flat branch of F. Therefore, inside this subregion the 2-cycle is superstable, outside is only stable.

To mark the border of the magenta region, there is another border collision curve given by $F^2(\eta_3) = \eta_3$. At this curve a periodic point of the locally-asymptotically stable 2-cycle that we observe only in the magenta region has a contact with the kink point η_3. Exiting the magenta region by crossing this curve, a border-collision bifurcation through which the 2-cycle disappear and either a stable cycle of a higher periodicity, or a chaotic attract, appears. We observe, for example, a locally-asymptotically stable 3-cycle, 4-cycle, and 5-cycle, see the enlargement of the parameter space in Fig. 8b. However, many other cycles exist. An example of a 3-cycle of F is depicted in Fig. 9a. Crossing the border-collision bifurcation curve $F(\eta_3) = x_1^*$ and entering the green region, these attractors (either cycles or chaotic sets) disappear.

Another bifurcation curve is given by $F_2^{'} = -1$ or, equivalently, $\gamma_2 = 2b_2/r$. This curve marks the border between the orange region and the light-magenta region. Crossing this curve, a degenerate (border-collision) period-doubling bifurcation [also known as degenerate flip bifurcation, see Sushko et al. (2016) and Avrutin et al. (2019)] occurs through which the unique and globally stable equilibrium x_2^* losses stability and a 2-cycle appears, and is the unique attractor, entering the light-magenta region. Specifically, along this border the segment $[F(\eta_3), \eta_3]$ is filled with two-period cycles of F and η_3 is also a point of non-differentiability. Therefore, the 2-period cycle $\{F(\eta_3), \eta_3\}$ undergoes a border collision and persists (with symbolic sequence $\sigma_2\sigma_3$) entering the light-magenta region.[13] A point of the curve $F_2^{'} = -1$ is also a point of the curve $x_0^* = x_1^*$ and it is a border point of four regions: The orange one, the yellow one, the light-magenta one and the magenta one. At this point

[13] The support of map F is partitioned in at most five regions inside which F is linear: $I_0 = [0, \eta_1]$, $I_1 = (\eta_1, \eta_2]$, $I_2 = (\eta_2, \eta_3]$, $I_3 = (\eta_3, x_M]$ and $I_4 = (x_M, +\infty)$. Then, if F has an n-period cycle $\{x_1, x_2, \ldots, x_n\}$, we say that the cycle has symbolic sequence $\sigma_i\sigma_j, \ldots, \sigma_k$ when $x_1 \in I_i$, $x_2 \in I_j$ and $x_n \in I_k$, with $i, j, k \in \{0, 1, 2, 3, 4\}$

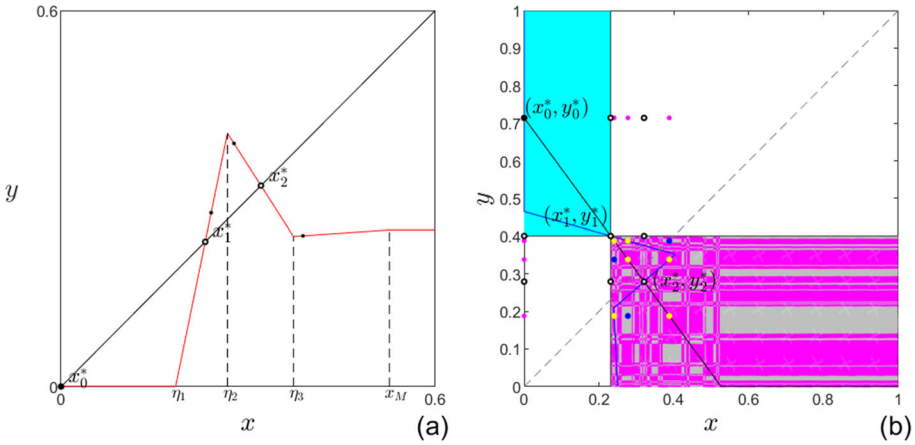

Fig. 9 **a** In red the graph of map F, stable fixed point as a black dot, unstable fixed point as empty black dot. **b** In cyan the basin of attraction of (x_0^*, y_0^*). In gray the basin of attraction of the 3-cycle depicted in blue. In magenta the basin of attraction of the 6-cycle depicted in yellow. In white the basin of attraction of the 6-cycle depicted in magenta. In blue the graph of $R_1(y)$, in black the graph of $R_2(x)$. Case 6(ii) in Proposition 3. Parameters: $a_1 = a_2 = 1, b_2 = 0.7, \gamma_2 = 1.9, \overline{b}_1 = 2, \underline{b}_1 = 0.3, \overline{\gamma}_1 = 2.15, \underline{\gamma}_1 = 0.2$. (Color figure online)

two bifurcations occur. The degenerate fold bifurcation at which x_0^* (superstable) and x_1^* (unstable) appear (increasing $\overline{\gamma}_1$) and the degenerate period-doubling bifurcation through which x_2^* loses stability and a locally-asymptotically stable 2-cycle appears. Moreover, the curve $F_2^{'} = -1$ marks the border between the yellow region and the magenta region. Even in this case a degenerate period-doubling bifurcation occurs through which x_2^* loses stability and a 2-period cycle appears which, however, is locally-asymptotically stable but not globally stable as it coexists with x_1^* (unstable) and x_0^* (superstable). In addition, the border-collision bifurcation curve $F_2^{'} = -1$ has a point of contact with another border collision curve given by $F(\eta_2) = \eta_3$. At this point, $\{\eta_2, \eta_3\}$ (the slope of F in (η_2, η_3) is -1) is a 2-period cycle, that is, the two kink points η_2 and η_3 are periodic points of the same cycle at the same time. Below this point, the curve $F_2^{'} = -1$ marks the border between the yellow region and the white region and identifies a bifurcation through which x_2^* loses stability and a chaotic attractor appears (increasing $\overline{\gamma}_1$). Specifically, at the border between the yellow region and the white region the segment $[\eta_2, F(\eta_2)]$ (instead of the segment $[F(\eta_3), \eta_3]$) is filled with 2-period cycles. Then, cycle $\{\eta_2, F(\eta_2)\}$ is the only one to undergo a border collision since its periodic point η_2 is the only one to be also a kink point. Due to this border collision, entering the white region only the 2-period cycle $\{\eta_2, F(\eta_2)\}$ persists and has symbolic sequence $\sigma_1\sigma_2$ (instead of $\sigma_2\sigma_3$ that we have entering the magenta region). Therefore, one period point of this cycle is in (η_1, η_2) while the other one is in (η_2, η_3). Leaving the yellow region and entering the white region, the slope of F is higher than one in the interval (η_1, η_2) (note that $x_1^* \in (\eta_1, \eta_2)$ is unstable). Moreover, the slope of F in (η_2, η_3) is smaller than -1 since in the white region we have $\overline{\gamma}_1 > 2b_2/r$. Therefore, the 2-period cycle of F with symbolic sequence $\sigma_1\sigma_2$ is unstable. A numerical analysis underlines that this 2-period cycle of F is surrounded by a two-piece chaotic attractor. Further increasing $\overline{\gamma}_1$ in the white region a one-piece chaotic attract emerges, see Fig. 10a for an example.

A further locus of bifurcation points is given by $F^2(\eta_2) = x_1^*$ at which an homoclinic bifurcation takes place. This bifurcation curve is made of two pieces. A piece of the curve

marks the border of the white region and the green region, crossing which the chaotic attractor of the white region becomes a repellor in the green region and almost all trajectories are attracted by x_0^*. The other piece of the homoclinic bifurcation curve is inside the green region. In the green region below this piece of curve a chaotic repellor exists.

The last border-collision curve that we comment is given by equation $x_2^* = x_1^*$ ($F(\eta_1) = \eta_1$). This curve identifies a persistent border-collision when it marks the border between the light-blue region and the orange region. In this locus of points x_2^* merges with x_1^* at the kink point η_1, x_2^* exists and is globally stable in the orange region, while x_1^* exists and is globally stable in the light-blue region. Moreover, this curve marks the border of the brown-yellow region and of the yellow region. At this locus of points a fold border-collision bifurcation occurs where equilibria x_1^* (unstable) and x_2^* (locally-asymptotically stable) appear entering the yellow region. They coexist with the superstable equilibrium x_0^* which is present in both regions. Furthermore, this curve marks the border of the brown-yellow region and of the white region. This locus of points identifies a degenerate fold-bifurcation at which equilibria x_1^* and x_2^* appear entering the white region and are both unstable. In addition to that, a chaotic attractor appears. Finally, the curve $x_1^* = x_2^*$ marks also the border between the brown-yellow region and the green region. At this boundary a fold-bifurcation occurs through which x_1^* and x_2^* appear entering the green region, they are both unstable, and a chaotic repellor also appears. The corner point of the green, white and brown-yellow region is the intersection point of the homoclinic bifurcation curve $F^2(\eta_2) = x_1^*$ and of the bifurcation curve $x_1^* = x_2^*$.

Ending the analysis of the two-dimensional bifurcation diagram of Fig. 8a, it is worth noting that entering the white region from the yellow, brown-yellow and green regions we have (or we may have) an abrupt transition from a stable equilibrium to chaotic dynamics. This is a peculiarity of piecewise smooth maps and it has relevant economic implications. Indeed, learning to forecast is limited in a chaotic regime and this justifies a duopoly where firms do not learn to play a Cournot–Nash equilibrium.

4.1.2 Scenarios 1: bifurcations and global dynamics of *T*

The global dynamics of map T inside the colored regions of the parameter space in Fig. 8a can be deduced by the dynamics of F described above. To this aim, we remark that the existence of a 2-period cycle of F implies the existence of a 4-period cycle of T, the existence of two stable equilibria of F implies the existence of two stable equilibria of T but also of a stable 2-cycle of T, see Proposition 4 for more details. Having made these remarks, we start commenting the dynamics of T inside the colored regions of the bifurcation diagram of Fig. 8a.

Looking at the two-dimensional bifurcation diagram of Fig. 8a, we have that (x_0^*, y_0^*) is the unique and globally stable equilibrium in the brown-yellow region, (x_3^*, y_3^*) is the unique and globally stable equilibrium in the light-green region, (x_1^*, y_1^*) is the the unique and globally stable equilibrium in the light-blue region and (x_2^*, y_2^*) is the the unique and globally stable equilibrium in the orange region.

The light-magenta region is also a region of the parameter space characterized by a unique equilibrium given by (x_2^*, y_2^*), which however is unstable. This equilibrium is surrounded by a 4-cycle which is globally stable.[14]

The remaining regions are characterized by three equilibria and by three 2-period cycles. It is the case of the gray region where the equilibria are (x_0^*, y_0^*) (superstable), (x_1^*, y_1^*) (unstable) and (x_3^*, y_3^*) (locally-asymptotically stable). Moreover, the 2-cycles are

[14] By global stability 4-cycle we mean a cycle that attracts all sets of points excluding those of zero measure.

$\left\{\left(x_0^*, y_3^*\right), \left(x_3^*, y_0^*\right)\right\}$ (superstable), $\left\{\left(x_0^*, y_1^*\right), \left(x_1^*, y_0^*\right)\right\}$ (saddle) and $\left\{\left(x_1^*, y_3^*\right), \left(x_3^*, y_1^*\right)\right\}$ (saddle), see Proposition 4(i)–(ii). The yellow region where the equilibria are $\left(x_0^*, y_0^*\right)$ (superstable), $\left(x_1^*, y_1^*\right)$ (unstable) and $\left(x_2^*, y_2^*\right)$ (locally-asymptotically stable). Moreover, the 2-cycles are $\left\{\left(x_0^*, y_2^*\right), \left(x_2^*, y_0^*\right)\right\}$ (superstable), $\left\{\left(x_0^*, y_1^*\right), \left(x_1^*, y_0^*\right)\right\}$ (saddle) and $\left\{\left(x_1^*, y_2^*\right), \left(x_2^*, y_1^*\right)\right\}$ (saddle), see Proposition 4(i)–(ii). The white region where there are the same equilibria and the same 2-cycles but $\left(x_2^*, y_2^*\right)$ is unstable, $\left\{\left(x_0^*, y_2^*\right), \left(x_2^*, y_0^*\right)\right\}$ is a saddle and $\left\{\left(x_1^*, y_2^*\right), \left(x_2^*, y_1^*\right)\right\}$ is unstable, see Proposition 4(i)–(ii).

Moreover, numerical simulation of Fig. 10b confirms the existence of two chaotic attractors. Specifically, we observe that the 2-cycle $\left\{\left(x_0^*, y_2^*\right), \left(x_2^*, y_0^*\right)\right\}$ is surrounded by a two-piece chaotic attractor which is denoted by $\mathcal{C}_1$. This two-piece chaotic attractor coexists with the one-piece chaotic attractor denoted by $\mathcal{C}_2$ and originated when $\left(x_2^*, y_2^*\right)$ losses stability. These two chaotic attractors coexist with the superstable equilibrium $\left(x_0^*, y_0^*\right)$. Looking at the basins of these three attractors, we observe that they are disconnected. This occurs as the map T is non-invertible. Economically speaking, this means that we can jump from a region where one firm dominates the market (its level of production is higher than the one of the competitor) to a region where the firm is out of the market (its level of production is zero). These chaotic attractors become unstable in the green region, where we have the unique (almost) globally attracting equilibrium $\left(x_0^*, y_0^*\right)$ that coexists with the unstable equilibria $\left(x_1^*, y_1^*\right)$ and $\left(x_2^*, y_2^*\right)$ and with the 2-cycles $\left\{\left(x_0^*, y_2^*\right), \left(x_2^*, y_0^*\right)\right\}$ (saddle), $\left\{\left(x_0^*, y_1^*\right), \left(x_1^*, y_0^*\right)\right\}$ (saddle) and $\left\{\left(x_1^*, y_2^*\right), \left(x_2^*, y_1^*\right)\right\}$ (unstable).

Finally, we have the regions in magenta, red, azure, green and so on, that are characterized by a cycle of periodicity 4, 6, 8, 10 and so on, that surrounds $\left(x_2^*, y_2^*\right)$. Moreover, a second locally-asymptotically stable cycle of periodicity 4, 6, 8, 10 and so on exists and surrounds the unstable two cycle $\left\{\left(x_0^*, y_2^*\right), \left(x_2^*, y_0^*\right)\right\}$. These cycles are stable and coexist with the stable equilibrium $\left(x_0^*, y_0^*\right)$, with the unstable equilibria $\left(x_1^*, y_1^*\right)$ and $\left(x_2^*, y_2^*\right)$, and with the related 2-cycles. For example, entering the magenta region from the yellow region, $\left(x_2^*, y_2^*\right)$ losses stability and a stable 4-cycle appears. At the same time, $\left\{\left(x_0^*, y_2^*\right), \left(x_2^*, y_0^*\right)\right\}$ looses stability and a second stable 4-cycle appears. Entering the red regions, instead of these two stables 4-cycle we have two stable 6-cycles. See Fig. 9 for an example of a stable 6-cycle of map T (basin of attraction in magenta) that surrounds the equilibrium $\left(x_2^*, y_2^*\right)$. This cycle coexists with a stable 3-cycle that also surrounds the equilibrium $\left(x_2^*, y_2^*\right)$ and its basin of attraction is depicted in gray. We observe that the basins of attraction of these two cycles are disconnected. Moreover, we have a second stable 6-cycle and the equilibrium $\left(x_0^*, y_0^*\right)$ that is also stable.

In terms of bifurcations, we just mention some peculiarity related to map T. Specifically, crossing the vertical line $x_0^* = x_1^*$ by entering the gray region a saddle-node border collision bifurcation occurs through which $\left(x_1^*, y_1^*\right)$ (unstable) and $\left(x_3^*, y_3^*\right)$ (stable) appear as well as the 2-cycles $\left\{\left(x_0^*, y_1^*\right), \left(x_1^*, y_0^*\right)\right\}$ (saddle), $\left\{\left(x_0^*, y_3^*\right), \left(x_3^*, y_0^*\right)\right\}$ (superstable) and $\left\{\left(x_1^*, y_3^*\right), \left(x_3^*, y_1^*\right)\right\}$ (saddle). A similar bifurcation occurs crossing the vertical line $x_0^* = x_1^*$ and entering the yellow region. The only difference is the equilibrium $\left(x_2^*, y_2^*\right)$ that appears instead of $\left(x_3^*, y_3^*\right)$ and the 2-cycles $\left\{\left(x_0^*, y_2^*\right), \left(x_2^*, y_0^*\right)\right\}$ (superstable) and $\left\{\left(x_1^*, y_2^*\right), \left(x_2^*, y_1^*\right)\right\}$ (saddle) that appear instead of $\left\{\left(x_0^*, y_3^*\right), \left(x_3^*, y_0^*\right)\right\}$ (superstable) and $\left\{\left(x_1^*, y_3^*\right), \left(x_3^*, y_1^*\right)\right\}$ (saddle).

Crossing instead the bifurcation curve $F_2^{'} = -1$ at the border between the orange region and the light-magenta region, the map T is such that the square with vertices given by the periodic points of the following cycle

$$\left\{\left(\eta_3, R_2\left(\eta_3\right)\right), \left(F\left(\eta_3\right), R_2\left(\eta_3\right)\right), \left(F\left(\eta_3\right), R_2\left(F\left(\eta_3\right)\right)\right), \left(\eta_3, R_2\left(F\left(\eta_3\right)\right)\right)\right\} \tag{35}$$

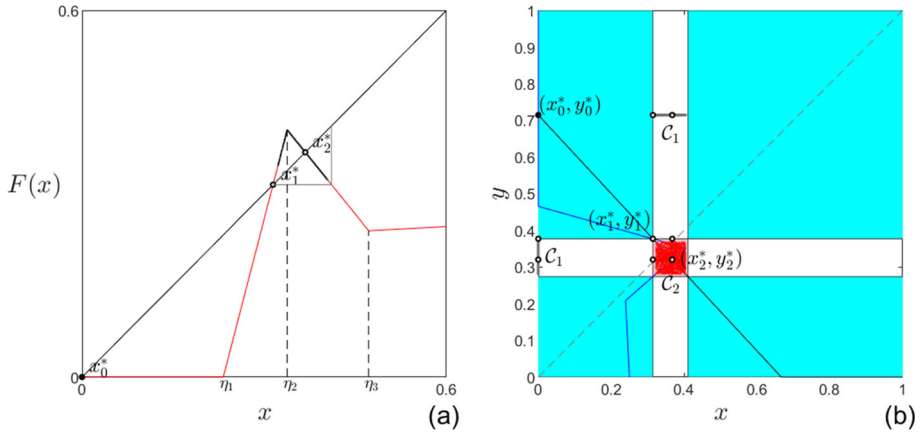

Fig. 10 **a** In red the graph of map F, stable fixed point as a black dot, unstable fixed point as empty black dot. **b** In dark gray the 2-pieces chaotic attractor $\mathcal{C}_1$. In red the one-piece chaotic attractor $\mathcal{C}_2$. In cyan the basin of attraction of $\left(x_0^*, y_0^*\right)$. In white the basin of attraction of $\mathcal{C}_1$. In pink the basin of attraction of $\mathcal{C}_2$. In blue the graph of $R_{\underline{1}}(y)$, in black the graph of $R_2(x)$. Case 6(ii) in Proposition 3. Parameters: $a_1 = a_2 = 1, b_2 = 0.7$, $\gamma_2 = 1.5, \overline{b}_1 = 2, \underline{b}_1 = 0.3, \overline{\gamma}_1 = 2.15, \underline{\gamma}_1 = 0.2$. (Color figure online)

is filled with four-period cycles that are marginally stable. Moreover, only the four-period cycle in (35) persists inside the light-magenta region and is the unique attractor. To be more specific, the four-period cycle for T persists both in the light-magenta region [Case 10(ii)] and in the magenta region [inside Case 6(ii)]. However, a border-collision bifurcation occurs by crossing the border of the light-magenta region and entering the magenta region. Indeed, at this border the equilibria $\left(x_0^*, y_0^*\right)$ and $\left(x_1^*, y_1^*\right)$ merge in the point of discontinuity $(\eta_1, R_2(\eta_1))$ and persists in the magenta region, where $\left(x_0^*, y_0^*\right)$ is super stable while $\left(x_1^*, y_1^*\right)$ is unstable. In the magenta region we also have the 2-cycles $\left\{\left(x_0^*, y_1^*\right), \left(x_1^*, y_0^*\right)\right\}$, $\left\{\left(x_0^*, y_2^*\right), \left(x_2^*, y_0^*\right)\right\}$ and $\left\{\left(x_1^*, y_2^*\right), \left(x_2^*, y_1^*\right)\right\}$ that appear entering this region and persist inside it.

Crossing the same curve $F_2' = -1$ but at the border between the yellow region and the magenta region, the equilibrium $\left(x_2^*, y_2^*\right)$ and the two-period cycle $\left\{\left(x_0^*, y_2^*\right), \left(x_2^*, y_0^*\right)\right\}$ lose stability as one of the associated eigenvalues becomes smaller than -1. At the bifurcation, the square with vertices given by the periodic points of the four-period cycle (35) is filled with marginally stable 4-period cycles, as it is when the border between the orange and the light-magenta regions is crossed. Differently from that case, here we also have the segments $\left\{(x, y) | \, y = y_0^* \text{ and } x \in [F(\eta_3), \eta_3]\right\}$ filled with two periodic points and the segment $\left\{(x, y) | \, x = x_0^* \text{ and } y \in [R_2(\eta_3), R_2(F(\eta_3))]\right\}$ filled with other two periodic points of 4-period cycles.

The remaining bifurcations and border collisions that regulate the change in the dynamics crossing regions will not be discussed for map T as they are already explained by analyzing the dynamics of F.

4.2 Scenario 2

Let us return to the dynamics of map F. An interesting feature of the dynamics of this map is the stability of their cycles. Looking at the bifurcation diagram of Fig. 8a, we observe that some cycles have a periodic point that involves the flat branch F_4 of F and are therefore

superstable. All the other cycles have instead a periodic point that involves also the branch F_3 of F. Setting $\underline{\gamma}_1 = 0$, branch F_3 is flat (zero slope) and coincides with the branch F_4. Then, any cycle has a periodic point in a flat region and is *superstable* (the associated eigenvalue is zero).

To investigate this peculiar case, let us consider a second configuration of the values of the non-bifurcation parameters given by

$$\overline{b}_1 = 2, \quad \underline{b}_1 = 0.3, \quad b_2 = 0.7, \quad \underline{\gamma}_1 = 0, \tag{36}$$

This set of values is as the one in (34) but $\underline{\gamma}_1 = 0$.

Then, we consider the two-dimensional bifurcation diagram of Fig. 11a obtained varying $\overline{\gamma}_1$ in $\left(\underline{\gamma}_1, 3\right) = (0, 3)$ and γ_2 in $(0, 3)$ and we first analyze the dynamics of F and later the one of T by focusing on the differences with the previous scenario.

4.2.1 Scenario 2: the dynamics of *F*

Investigating the two-dimensional bifurcation diagram of Fig. 11a, we observed a first relevant difference with the two-dimensional bifurcation diagram of Fig. 8a. Specifically, we observe that the white region indicating chaotic attractors is shrunk and is now bounded by the border-collision bifurcation curves given by $x_1^* = x_2^*$ from below, by $F_2^{'} = -1$ on the left, by $F^2(\eta_2) = x_1^*$ on the right and by $F(\eta_2) = \eta_3$ from above. This last border of the white region was not present in the previous two-dimensional bifurcation diagram obtained with a positive $\underline{\gamma}_1$, compare Fig. 8a, 11a.

A second relevant difference is the lower border of the region of periodic cycles. Starting in the magenta region there is a 2-cycle, which is now superstable. Then, reducing the value of γ_2, we now observe border-collision bifurcations through which superstable cycles of different periodicity appear, but never chaos as long as we are above the curves $F(\eta_2) = \eta_3$ and $F^2(\eta_2) = x_1^*$. Specifically, the lower boundary of the region of superstable cycles is marked by these two curves.

Regarding the first bifurcation curve $F(\eta_2) = \eta_3$, we have that all periodic dynamics above this curve have a periodic point that involves the flat branch F_3 of F and cycles are therefore superstable. Below the bifurcation curve $F(\eta_2) = \eta_3$, all attractors different from an equilibrium do not involve the flat branch F_3 and chaotic dynamics are observed.

Regarding instead the homoclinic bifurcation curve $F^2(\eta_2) = x_1^*$, we have that this curve marks the border between the region of superstable cycles and the green region. Specifically, crossing from above this curve we enter the green region where a chaotic repellor can be detected. In the two-dimensional bifurcation diagram of Fig. 8a, the upper-boundary of the green region coincides instead with the border-collision bifurcation curve $F(\eta_3) = x_1^*$.

Except for the existence of superstable cycles that substitute chaotic dynamics and/or non-superstable cycles above the bifurcation curves $F(\eta_2) = \eta_3$ and $F(\eta_3) = x_1^*$, the two-dimensional bifurcation diagram of Fig. 11a is analogous to the one of Fig. 8a.

4.2.2 Scenario 2: the dynamics of *T*

Setting $\underline{\gamma}_1 = 0$, the dynamics of T changes as well. Indeed, excluding the yellow region, in all the other regions where there is a stable cycle, this cycle is also superstable. It is the case of the 2-cycle $\left\{\left(x_0^*, y_3^*\right), \left(x_3^*, y_0^*\right)\right\}$ in the gray region, the 4-cycle in the light-magenta region, the two 4-cycles in the magenta region and so on.

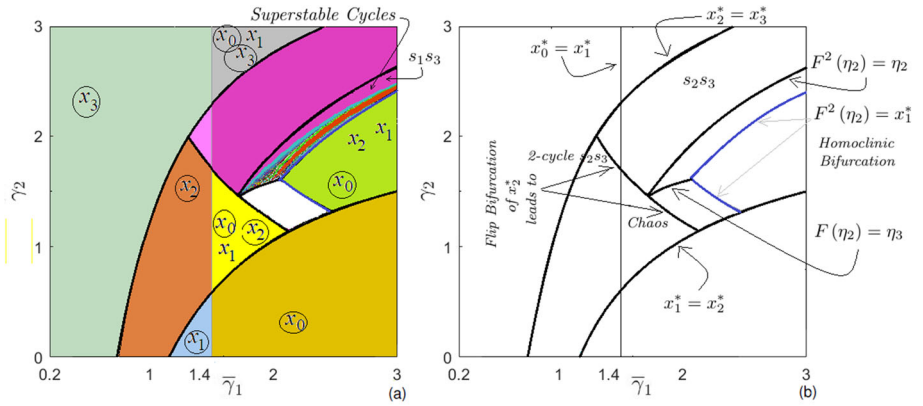

Fig. 11 Two-dimensional bifurcation diagrams showing the bifurcation curves for the super stable cycles in the parameter plane $\overline{\gamma}_1 - \gamma_2$. **a** $(\overline{\gamma}_1, \gamma_2) \in [0.2, 3] \times [0, 3]$. **b** $(\overline{\gamma}_1, \gamma_2) \in [1.2, 3] \times [1.2, 3]$. Remaining parameters as in (36). The equilibria x_i^* are indicated as x_i for the sake of simplicity of notation. (Color figure online)

Moreover, also for map T we have that attracting chaotic dynamics are confined to the white region below the bifurcation curve $F(\eta_2) = \eta_3$, while in the green region there are chaotic repellors. We remark that the existence of a chaotic invariant set of T implies always the existence of also a second chaotic invariant set.

4.3 Scenario 3

So far, we have not consider parameter configurations that include the Case 5(i) and (ii) of Proposition 3. In order to underline the dynamics under these two specific cases, let us consider the following new set of values of the non-bifurcation parameters:

$$\overline{b}_1 = 2, \quad \underline{b}_1 = 0.05, \quad b_2 = 0.09, \quad \underline{\gamma}_1 = 0.2, \tag{37}$$

Then, the parameter plane $(\overline{\gamma}_1, \gamma_2)$ of Fig. 12, where $\overline{\gamma}_1$ varies in $(\underline{\gamma}_1, 3)$ and γ_2 varies in $(0, 3)$, shows the cases identified in Proposition 3.

4.3.1 Scenario 3: the dynamics of *F*

Looking at the dynamics of F, one of the main difference with respect to the previous scenarios is the presence of Cases 5(i) (violet region in the two-dimensional bifurcation diagram of Fig. 13) and Case 5(ii) (light-azure region in the two-dimensional bifurcation diagram of Fig. 13). Respect to Cases 6(i), in Case 5(i) we have three locally-asymptotically stable equilibria, that is x_0^* (superstable), x_2^* (stable) and x_4^* (superstable). This is the only case in which three stable equilibria coexist. A numerical example showing the three coexisting stable equilibria is reported in Fig. 14a.

Respect to Case 6(ii), moreover, in Case 5(ii) we can have an attractor (either chaotic or periodic) that coexists with two superstable equilibria, that is x_0^* and x_4^*, instead of coexisting with the superstable equilibrium x_0^* only. In this respect, the two-dimensional bifurcation diagram of Fig. 13a underlines that only chaotic dynamics coexists with the stable equilibria x_0^* and x_4^* in the region identifying Case 5(ii).

A second peculiarity that we observe in the two-dimensional bifurcation diagram of Fig. 14a is the border-collision bifurcation curve $x_3^* = x_4^*$ that marks the borders between Cases 6(ii) and 5(ii) and between Cases 6(i) and 5(i). This locus of points identifies a degenerate fold bifurcation as crossing this curve and entering either Case 5(i) or Case 5(ii), we have that the two equilibria x_3^* and x_4^* merge at the kink point η_3. Above this curve, the equilibrium x_3^* is unstable while x_4^* is superstable.

A third peculiarity is the bifurcation through which x_2^* losses stability, which leads to either a chaotic dynamics or to a chaotic repellor. Therefore, we have always an abrupt transition from the asymptotically-stable equilibrium x_2^* to chaos, that is, we never have a transition from the asymptotically-stable equilibrium x_2^* to attracting cycles as it was possible in the two previous bifurcation diagrams. Specifically, the stable cycles do not appear when x_2^* losses stability. Note that the bifurcation curve $F_2^{'} = -1$ marks the border of the white region and of the either yellow or violet region or, alternatively, it marks the border of the either yellow or violet region and of the green region. This last case also represents a novelty. Indeed, in the previous two bifurcation diagrams there were no direct transaction from a stable x_2^* to a chaotic repellor. Therefore, this last numerical observation confirms the three possible dynamics indicated in Proposition 3 that can appear when x_2^* losses stability, that is, an attracting cycle, a chaotic attractor and a chaotic repellor.

Despite periodic orbits do not appear when x_2^* losses stability, they may appear through a different border-collision bifurcation and one periodic point of all these cycles involves always the flat branch F_4 of F. Therefore, all cycles are superstable. Specifically, the periodic solutions are confined above by the border-collision bifurcation curve $F^2(\eta_3) = x_M$ at which the unique periodic point of a cycle that is in the region where F is flat has a contact with the kink-point x_M and above this curve the periodic point enters the interval (η_3, x_M) where F is not flat anymore and chaotic dynamics emerge.

Moreover, the region of stable periodic solutions is bounded below by the homoclinic bifurcation curve $F^2(\eta_2) = x_1^*$. Below this bifurcation curve, almost all trajectories are absorbed by the superstable equilibrium x_0^*.

As a further relevant difference, we note that increasing γ_2 and crossing the border of the brown-yellow region, we never enter the white region where there is a chaotic attractor but only a region where the superstable equilibrium x_0^* attracts all transitory dynamics.

4.4 Scenario 4

The parameter configurations considered so far show that periodic solutions and chaos occur when $\overline{\gamma}_1 > \underline{b}_1$ and $\gamma_2 > b_2$. As discussed in Radi and Gardini (2023), when these conditions apply the parameter realizations $(\underline{b}_1, \overline{\gamma}_1)$ and (b_2, γ_2) are justified by assuming that a player consider that further competitors can potentially enter the market in the next period. Here, we show for the first time that periodic and chaotic dynamics are also possible under parameter realizations consistent with a duopoly game without threat of new entry, that is $\overline{\gamma}_1 \leq \underline{b}_1$ and $\gamma_2 \leq b_2$.

As illustration, Fig. 15a show the existence of a stable 4-cycle, denoted by $\mathcal{C}_4$, for the following constellation of parameters, that is

$$\overline{b}_1 = 1.2, \quad \underline{b}_1 = 0.9, \quad \overline{\gamma}_1 = 0.9, \quad \underline{\gamma}_1 = 0, \quad b_2 = 1.4, \quad \gamma_2 = 1.4. \tag{38}$$

which is consistent with Case 10(ii) of Proposition 3.

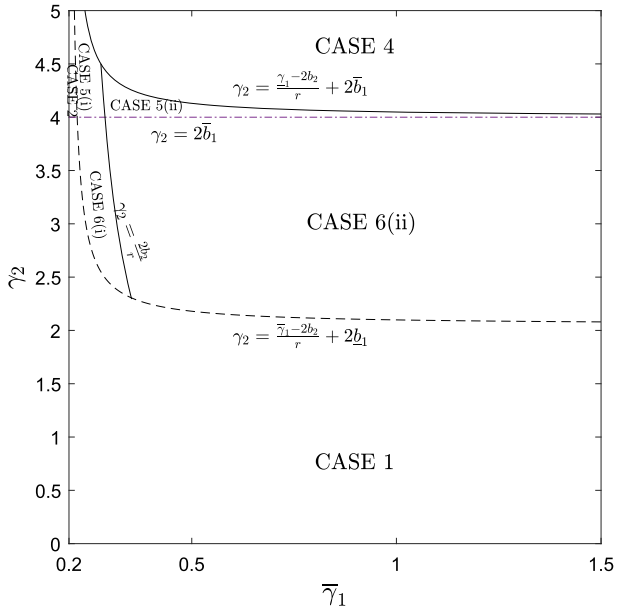

Fig. 12 Parameter plane $\overline{\gamma}_1 - \gamma_2$ showing the borders of the regions representing the cases identified in Proposition 3. Parameters: $(\overline{\gamma}_1, \gamma_2) \in [0.2, 1.5] \times [0, 5]$ and the remaining ones as in (37)

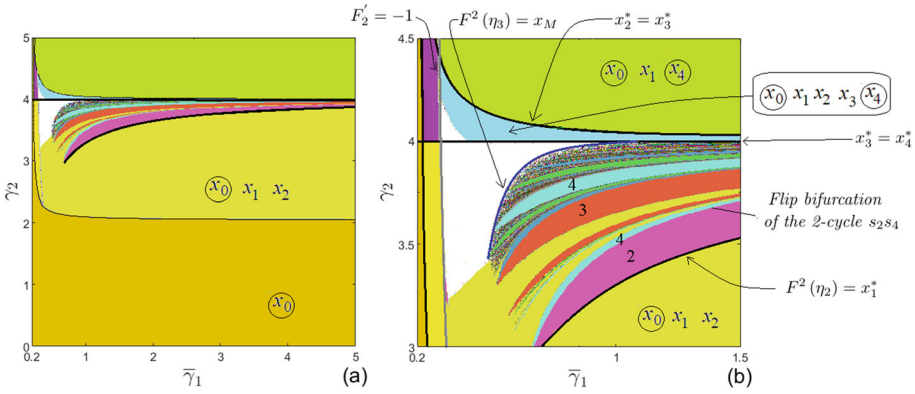

Fig. 13 Two-dimensional bifurcation diagrams showing the bifurcation curves (see Proposition 3) in the parameter plane $\overline{\gamma}_1 - \gamma_2$ for $(\overline{\gamma}_1, \gamma_2) \in [0.2, 3] \times [0, 3]$. Remaining parameters as in (37). The equilibria x_i^* are indicated as x_i for the sake of simplicity of notation

As illustration of the chaotic dynamics possible, Fig. 15b shows the existence of a chaotic attractor, denoted by $\mathcal{C}_5$, when the values of the parameters are as follows:

$$\overline{b}_1 = 1.1, \quad \underline{b}_1 = 0.99, \quad \overline{\gamma}_1 = 0.99, \quad \underline{\gamma}_1 = 0.06, \quad b_2 = 1.71, \quad \gamma_2 = 1.7. \tag{39}$$

This constellation of parameters is also consistent with Case 10(ii) of Proposition 3.

Chaotic attractors can even coexist as shown in Fig. 15c, where

$$\overline{b}_1 = 1.1, \quad \underline{b}_1 = 0.99, \quad \overline{\gamma}_1 = 0.99, \quad \underline{\gamma}_1 = 0.09, \quad b_2 = 1.71, \quad \gamma_2 = 1.7. \tag{40}$$

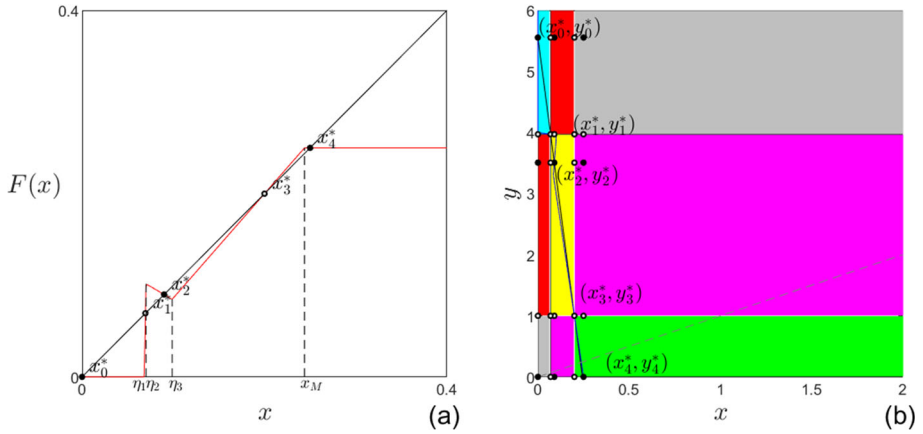

Fig. 14 **a** In red the graph of map F, stable fixed point as a black dot, unstable fixed point as empty black dot. **b** In cyan the basin of attraction of $\left(x_0^*, y_0^*\right)$. In yellow the basin of attraction of $\left(x_2^*, y_2^*\right)$. In green the basin of attraction of $\left(x_4^*, y_4^*\right)$. In gray the basin of attraction of the 2-cycle $\left\{\left(x_0^*, y_4^*\right); \left(x_4^*, y_0^*\right)\right\}$. In magenta the basin of attraction of the 2-cycle $\left\{\left(x_2^*, y_4^*\right); \left(x_4^*, y_2^*\right)\right\}$. In red the basin of attraction of the 2-cycle $\left\{\left(x_0^*, y_2^*\right); \left(x_2^*, y_0^*\right)\right\}$. In blue the graph of $R_1\,(y)$, in black the graph of $R_2\,(x)$. Case 5(i) in Proposition 3. Parameters: $\gamma_2 = 4.1$, $\overline{\gamma}_1 = 0.25$, and the remaining ones as in (37)

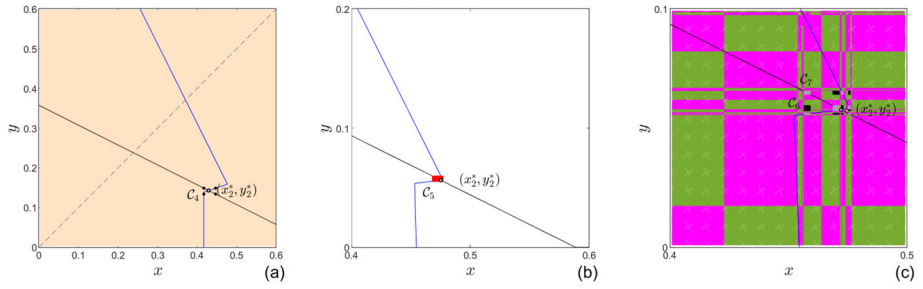

Fig. 15 In bisque the basin of attraction of the 4-cycle $\mathcal{C}_4$. In white the basin of attraction of the chaotic attractor $\mathcal{C}_5$, which is depicted in red. In brown green the basin of attraction of the chaotic attraction $\mathcal{C}_6$, which is depicted in black. In magenta the basin of attraction of the chaotic attraction $\mathcal{C}_7$, which is depicted in gray. **a** Parameters as in (38). **b** Parameters as in (39). **c** Parameters as in (40)

The basins of attraction of the coexisting chaotic attractors are disconnected, showing that all the possible form of complexity observed in the model occurs also for parameters constellations such that $\underline{b}_1 \geq \overline{\gamma}_1$ and $b_2 \geq \gamma_2$. Therefore, the current work extends the findings of Radi and Gardini (2023), showing that chaotic attractors, coexistence, and disconnected basins of attractions, emerge even in a parameter configuration consistent with a duopoly model without threat of new entry.

5 Economic implications

Our analysis confirms the counter-intuitive result that the conservative approach to uncertainty may lead to a very volatile output dynamics in a duopoly market populated by firms with constant expectations. The volatility in the output dynamics impacts on the market shares of

firms which are also volatile. This has several economic implications. Indeed, it is well know that the market shares of firms and their volatility impact on the level and type of investments (e.g., in general innovations versus in R&D innovations), see Comin and Philippon (2005) and Comin and Mulani (2009). Furthermore, the worst-case approach to uncertainty may lead to coexisting Nash equilibria, each of which is associated with a different level of production. Ending up in a Nash equilibrium which implies lower levels of production impacts on the rate of profit and on the consumer surplus, see, e.g., Sakai (1985), Huang (2008) and Lagerlöf (2007).

The volatility in the output dynamics is caused by either periodic orbits or chaotic dynamics that are originated by the strategic behavior. A peculiarity of our model is that chaotic dynamics are present for a large variety of parameter configurations and can suddenly emerge when a Nash equilibrium loses stability. This is the so-called robust chaos, that emerges only in non-smooth systems as featured in our duopoly model, see, e.g., Avrutin et al. (2019). Smooth systems generate instead narrow instances of chaos sensitive to parameter perturbations.

The just outlined chaotic dynamics of the strategic behavior and the randomness in the inverse-demand parameters causes price volatility. As underlined in Nocetti and Smith (2011), this goods-price volatility impacts on consumers' attitudes inducing, for example, precautionary saving. The price volatility can also lead consumers to seek to favorably time their purchases. Moreover, the volatility in the price dynamics and the volatility in the output dynamics combine and generates profit volatility. The persistent volatility in the profit dynamics can have several economic implications, for example in terms of (1) investments in R&D, advertising and capital expenditures, see, e.g., Czarnitzki and Toole (2011), Carruth et al. (2000) and Cho (1998), Caballero (1991) and Pindyck (1998); (2) costs of financing and access to the capital market, see, e.g., Minton and Schrand (1999).

Profit uncertainty is also enhanced by the deviation between anticipated and realized strategic behavior of the opponent. This further source of uncertainty is inherent to the chaotic dynamic regimes. Indeed, in a chaotic regime, firms may experience profits below their minimum expected payoffs due to incorrect anticipation of their opponent's strategic behavior. The economic implications are unexpected losses that impact on the financial stability of the duopoly, with obvious negative consequences in terms of investments, cost of debt and so no.

In addition, our results underline that chaotic dynamics can coexist with stable Nash equilibria for which basins of attraction are disconnected, and these features persist in a very large region of the parameter space. Therefore, the price dynamics of the duopoly may be very sensitive to perturbations in the level of productions. We can conclude that the price and profit dynamics can be very difficult to predict in a duopoly game with players engaged in robust optimization and adopting constant expectations concerning competitor production. Among the many possible economic implications of this, it is well known that the reduction of earnings predictability discourages investments (e.g. R&D investments), see, e.g., Minton and Schrand (1999) and Caballero (1991).

In summary, the worst-case approach to uncertainty in a Cournot duopoly model with constant expectations does not only modify the solution of the game from a single Nash equilibrium to potentially multiple equilibria, but it also reduces its stability region inside which players learn a Nash solution. Moreover, it causes volatility that it is by far larger than that which can be generated by the same model but without uncertainty. As discussed, these findings have several economic implications in terms of investment rates, cost of financing, consumers' behavior, consumers' surplus. Let us remark that all these aspects are not modeled in our duopoly game, but are just possible consequences of the higher volatility and the lower

predictability of prices, profits and level of productions that are experienced in a duopoly market where the inverse demands are uncertain and firms are engaged in robust optimization and have constant expectations concerning competitor production.

Despite some possible drawbacks when combined with constant expectations, we underline that the robust optimization approach to uncertainty offers several advantages, among which: (1) accommodating ambiguity aversion, see, e.g., Ellsberg (1961); (2) hedging against extreme events that are instead washed out by the expected value operator, see, e.g., Ben-Tal et al. (2009); (3) designing solution approaches that are immune to data uncertainty which can make the usual (stochastic) optimal solution completely meaningless from a practical viewpoint, see, e.g., Bertsimas and Sim (2004); (4) tractability and significant computational benefits, see, e.g., Keith and Ahner (2021).

6 Conclusions

The paper focuses on the global dynamics of a duopoly game where firms adopt constant expectations and are adverse to ambiguity. Ambiguity regards the possible realizations of the parameters of the inverse demand functions. Attention is paid on the bifurcations taking place when the firms' beliefs about the uncertainty sets are perturbed.

The investigation reveals that chaotic dynamics can emerge as the result of extreme ambiguity aversion and the inability to anticipate opponent's strategy. The emergence of a chaotic regime depends on the configuration of the uncertainty sets. Chaos is not observable when the uncertainty sets of the players of the duopoly are made of only a single worst-case realization. It emerges in a symmetric setup when the uncertainty sets of players are made of two worst-case realizations, see Radi and Gardini (2023). Here, we add to this literature by showing that chaos is observed even in the simpler setting where only one of the two players has an uncertainty set consisting of two worst-case realizations. Additionally, we also have coexistence between a chaotic attractor and a stable equilibrium whereas in Radi and Gardini (2023) a chaotic attract cannot coexists with a stable equilibrium. Finally, the asymmetry in worst-case beliefs introduces chaotic dynamics to the traditional duopoly configuration, an outcome that is not feasible in the symmetric game considered by Radi and Gardini (2023).

This is only a first step in studying the effect of asymmetric beliefs on the worst-case realizations of the uncertain values of the parameters of the duopoly game. Indeed, a more general investigation would imply to assume that both players have an uncertainty set made of two worst-case realizations. However, this will lead to a map F with up to eight branches. A further interesting extension of the current work would be to study the dynamics of the duopoly model under more general configurations of the uncertainty sets. For example, Goerigk and Schöbel (2016) summarizes six common uncertainty sets used in robust optimization. These tasks are left for a future research.

Acknowledgements This paper greatly benefited from the comments and suggestions of two anonymous referees and seminar participants at many universities and conference. Davide Radi acknowledges the financial support from the Czech Science Foundation under project 23-06282S, and an SGS research project of VSB-TUO (SP2023/19).

Author Contributions Davide Radi: Model development, Formal analysis, Investigation, Methodology, Writing—review & editing. Gardini Laura: Formal analysis, Methodology. David Goldbaum: Formal analysis, Writing—review & editing.

Funding Open access funding provided by Università Cattolica del Sacro Cuore within the CRUI-CARE Agreement.

Declarations

Conflict of interest The authors declare that they do not have any conflict of interest.

Ethical approval This article does not contain any studies with human participants or animals performed by any of the authors.

Appendix A: Recap of results on square decoupled maps

Some results from Bischi et al. (2000). Consider the functions

$$F(x) = R_1 \circ R_2(x) \quad \text{and} \quad G(y) = R_2 \circ R_1(y) \tag{A.1}$$

Then, as shown in Bischi et al. (2000), the following properties hold

Proposition 5 *For each integer $k \geq 1$ and for each integer $n \geq 1$:*

- $T^{2k}(x, y) = \left(F^k(x), G^k(y)\right)$;
- $R_1 \circ G^k(y) = F^k \circ R_1(y)$;
- $R_2 \circ F^k(x) = G^k \circ R_2(x)$;
- *If $\{x_1, \ldots, x_n\}$ is an n-cycle of F then $\{y_1, \ldots, y_n\} = \{R_2(x_1), \ldots, R_2(x_n)\}$ is the conjugate n-cycle of G and $\{x_1, x_2, \ldots, x_n\} = \{R_1(y_n), R_1(y_1), \ldots, R_1(y_{n-1})\}$. The two conjugate cycles have the same stability property.*
- *If $\{y_1, \ldots, y_n\}$ is an n-cycle of G then $\{x_1, \ldots, x_n\} = \{R_1(y_1), \ldots, R_1(y_n)\}$ is the conjugate n-cycle of F and $\{y_1, y_2, \ldots, y_n\} = \{R_2(x_n), R_2(x_1), \ldots, R_2(x_{n-1})\}$. The two conjugate cycles have the same stability property.*

We know that any n-cycle C of T, of odd or even period n, is necessarily associated with a cycle of F and one of G say C_x and C_y respectively. Let us denote by $\mathcal{B}(C)$ the total basin of an attractor C. It is given by $\mathcal{B}(C) = \cap_{n=0}^{\infty} T^{-n}(\mathcal{B}_{im}(C))$, where $\mathcal{B}_{im}(C)$ is the immediate basin of C, made up of the connected components of the basin containing C. Analogously, for the one-dimensional map F we have $\mathcal{B}(C_x) = \cap_{n=0}^{\infty} F^{-n}(\mathcal{B}_{im}(C_x))$, where $\mathcal{B}_{im}(C_x)$ is the immediate 1-dimensional basin of C_x, along the x axis.

Moreover, the cycles of the two-dimensional map T are related to those of the one-dimensional maps F and G, according to the following result:

Proposition 6 *We have the following results:*

- *A point (x_i, y_i) is a periodic point of period n for T if and only if x_i and y_i are periodic points of F and G, respectively, of period n (if n is odd) or a divisor of n (if n is even).*
- *Let C be an attracting cycle of T associated with the cycles C_x and C_z of F, then*
  - $\mathcal{B}(C) \subseteq \left[\mathcal{B}(C_x) \cup \mathcal{B}(C_z)\right] \times R_2\left(\left[\mathcal{B}(C_x) \cup \mathcal{B}(C_z)\right]\right)$;
  - $\mathcal{B}_{im}(C) \subseteq \left[\mathcal{B}_{im}(C_x) \cup \mathcal{B}_{im}(C_z)\right] \times R_2\left(\left[\mathcal{B}_{im}(C_x) \cup \mathcal{B}_{im}(C_z)\right]\right)$ *and $\mathcal{B}_{im}(C)$ is made up of rectangles which include the points of C;*

- *For T, the image of a horizontal segment is a vertical segment and vice-versa;*
- *For T, the preimages of a horizontal segment, if any, are vertical segments and vice-versa;*
- *For any periodic point $P = (x, y)$ of the map T of period $n \geq 1$, the horizontal and vertical lines $y = y_1$ and $x = x_1$, issuing from P, are trapping sets for the map T^n.*
- *Any saddle cycle of T has stable and unstable sets formed by the union of segments which are parallel to the coordinates axes.*

References

Aghassi, M., & Bertsimas, D. (2006). Robust game theory. *Mahematical Programming, Series B, 107*, 231–273.

Arrow, K., & Hurwicz, L. (1972). An optimality criterion for decision making under ignorance. In C. Carter & J. Ford (Eds.), *Uncertainty and expectations in Economics* (pp. 1–11). Oxford: Blackwell.

Avrutin, V., Gardini, L., Sushko, I., & Tramontana, F. (2019). *Continuous and discontinuous piecewise-smooth one-dimensional maps: Invariant sets and bifurcation structures*. World Scientific.

Ben-Tal, A., El-Ghaoui, L., & Nemirovski, A. (2009). *Robust optimization*. Princeton University Press.

Bertsimas, D., Brown, D. B., & Caramanis, C. (2011). Theory and applications of robust optimization. *SIAM Review, 53*, 464–501.

Bertsimas, D., & Sim, M. (2004). The price of robustness. *Operations Research, 52*, 35–53.

Bischi, G. I., Mammana, C., & Gardini, L. (2000). Multistability and cyclic attractors in duopoly games. *Chaos, Solitons & Fractals, 11*, 543–564.

Caballero, R. J. (1991). On the sign of the investment-uncertainty relationship. *American Economic Review, 81*, 279–288.

Carruth, A., Dickerson, A., & Henley, A. (2000). What do we know about investment under uncertainty? *Journal of Economic Surveys, 14*, 119–153.

Cho, M.-H. (1998). Ownership structure, investment, and the corporate value: An empirical analysis. *Journal of Financial Economics, 47*, 103–121.

Comin, D., & Mulani, S. (2009). A theory of growth and volatility at the aggregate and firm level. *Journal of Monetary Economics, 56*, 1023–1042.

Comin, D., & Philippon, T. (2005). The rise in firm-level volatility: Causes and consequences. *NBER Macroeconomics Annual, 20*, 167–201.

Crespi, G. P., Kuroiwa, D., & Rocca, M. (2018). Robust optimization: Sensitivity to uncertainty in scalar and vector cases, with applications. *Operations Research Perspectives, 5*, 113–119.

Crespi, G.P., Radi D., & Rocca, M. (2023). Insights on the theory of robust games. *Computational Economics*. https://doi.org/10.1007/s10614-023-10486-0

Crespi, G. P., Kuroiwa, D., & Rocca, M. (2018). Robust optimization: Sensitivity to uncertainty in scalar and vector cases, with applications. *Operations Research Perspectives, 5*, 113–119.

Crespi, G. P., Radi, D., & Rocca, M. (2017). Robust games: Theory and application to a Cournot duopoly model. *Decisions in Economics and Finance, 40*, 177–198.

Czarnitzki, D., & Toole, A. A. (2011). Patent protection, market uncertainty, and R&D investment. *The Review of Economics and Statistics, 93*, 147–159.

Ellsberg, D. (1961). Risk, ambiguity, and the Savage axioms. *The Quarterly Journal of Economics, 75*, 643–669.

Gilboa, I., & Schmeidler, D. (1989). Maxmin expected utility with non-unique prior. *Journal of Mathematical Economics, 18*, 141–153.

Goerigk, M., & Schöbel, A. (2016). Algorithm engineering in robust optimization. In L. Kliemann & P. Sanders (Eds.), *Algorithm engineering: Selected results and surveys* (pp. 245–279). Springer.

Hammond, P. J. (1976). Changing tastes and coherent dynamic choice. *The Review of Economic Studies, 43*, 159–173.

Hey, J. D., & Lotito, G. (2009). Naive, resolute or sophisticated? A study of dynamic decision making. *Journal of Risk and Uncertainty, 38*, 1–25.

Huang, W. (2008). The long-run benefits of chaos to oligopolistic firms. *Journal of Economic Dynamics and Control, 32*, 1332–1355.

Huck, S., Norman, H.-T., & Oechssler, J. (1999). Learning in cournot oligopoly—An experiment. *Economic Journal, 109*, C80–C95.

Keith, A. J., & Ahner, D. K. (2021). A survey of decision making and optimization under uncertainty. *Annals of Operations Research, 300*, 319–353.

Lagerlöf, J. (2007). Insisting on a non-negative price: Oligopoly, uncertainty, welfare, and multiple equilibria. *International Journal of Industrial Organization, 25*, 861–875.
Lepore, J. J. (2012). Cournot outcomes under Bertrand–Edgeworth competition with demand uncertainty. *Journal of Mathematical Economics, 48*, 177–186.
Machina, M. J. (1989). Dynamic consistency and non-expected utility models of choice under uncertainty. *Journal of Economic Literature, 27*, 1622–1668.
Malueg, D. A., & Tsutsui, S. O. (1996). Duopoly information exchange: The case of unknown slope. *International Journal of Industrial Organization, 14*, 119–136.
Malueg, D. A., & Tsutsui, S. O. (1998). Oligopoly information exchange when non-negative price and output constraints may bind. *Australian Economic Papers, 37*, 363–371.
Mamatame, A., & Tse, E. (1981). Adaptive expectations and dynamic adjustment in noncooperative games with incomplete information. *Journal of Optimization Theory and Applications, 34*, 243–261.
Minton, B. A., & Schrand, C. (1999). The impact of cash flow volatility on discretionary investment and the costs of debt and equity financing. *Journal of Financial Economics, 54*, 423–460.
Nocetti, D., & Smith, W. T. (2011). Price uncertainty, saving, and welfare. *Journal of Economic Dynamics and Control, 35*, 1139–1149.
Pindyck, R. S. (1998). Irreversible investment, capacity choice, and the value of the firm. *American Economic Review, 78*, 969–85.
Radi, D., & Gardini, L. (2023). Ambiguity aversion as a route to randomness in a duopoly game. ArXiv:5228177
Radi, D., & Gardini, L. (2023). Border collision bifurcations in a piecewise linear duopoly model. *Journal of Difference Equations and Applications, Advance Online Publication.* https://doi.org/10.1080/10236198.2023.2203276
Rand, D. (1978). Exotic phenomena in games and duopoly models. *Journal of Mathematical Economics, 5*, 173–184.
Rocca, M. (2022). Sensitivity to uncertainty and scalarization in robust multiobjective optimization: An overview with application to mean-variance portfolio optimization. *Annals of Operations Research, Advance online publication.* https://doi.org/10.1007/s10479-022-04951-6
Rubinstein, A. (1991). Comments on the interpretation of game theory. *Econometrica, 59*, 909–924.
Sakai, Y. (1985). The value of information in a simple duopoly model. *Journal of Economic Theory, 36*, 36–54.
Singh, N., & Vives, X. (1984). Price and quantity competition in a differentiated duopoly. *The RAND Journal of Economics, 15*, 546–554.
Soyster, A. L. (1973). Convex programming with set-inclusive constraints and applications to inexact linear programming. *Operations Research, 21*, 1154–1157.
Sushko, I., Avrutin, V., & Gardini, L. (2016). Bifurcation structure in the skew tent map and its application as a border collision normal form. *Journal of Difference Equations and Applications, 22*, 1040–1087.
Vega-Redondo, F. (1997). The evolution of Walrasian behavior. *Econometrica, 65*, 375–384.
von Neumann, J., & Morgenstern, O. (1947). *Theory of games and economic behavior*. Princeton University Press.
Wald, A. (1945). Statistical decision functions which minimize the maximum risk. *Annals of Mathematics, 46*, 265–280.
Xu, J. (2010). Duopoly information sharing with differentiated products. *Operations Research Letters, 38*, 287–291.